CNRS UMR 6072

CNRS THEMATIC SCHOOL
PORT-BAIL - VVF CENTER
50580 PORT-BAIL
FRANCE

INTERNATIONAL SCIENTIFIC SCHOOL

HIGH SENSITIVITY MAGNETOMETERS "SENSORS & APPLICATIONS" NOVEMBER 4-8, 2002

SUPPORTED BY

EUROPEAN OFFICE OF R&D OF THE USAF
UNIVERSITY OF CAEN
CONSEIL REGIONAL DE LA REGION BASSE NORMANDIE

CNRS CENTRE NATIONAL DE LA RECHERCHE SCIENTIFIQUE

REPORT DOCUMENTATION PAGE

Form Approved OMB No. 0704-0188

1. REPORT DATE *(DD-MM-YYYY)*	2. REPORT TYPE	3. DATES COVERED *(From – To)*
31-01-2003	Conference Proceedings	4 November 2002 - 8 November 2002

4. TITLE AND SUBTITLE

High Sensitivity Magnetometers 'Sensors and Applications'

5a. CONTRACT NUMBER
F61775-02-WF077

5b. GRANT NUMBER

5c. PROGRAM ELEMENT NUMBER

6. AUTHOR(S)

Conference Committee

5d. PROJECT NUMBER

5d. TASK NUMBER

5e. WORK UNIT NUMBER

7. PERFORMING ORGANIZATION NAME(S) AND ADDRESS(ES)

University of Caen
Dept. Sciences Pour l'ingénieur
6, Bd du maréchal juin
CAEN, 14050
France

8. PERFORMING ORGANIZATION REPORT NUMBER

N/A

9. SPONSORING/MONITORING AGENCY NAME(S) AND ADDRESS(ES)

EOARD
PSC 802 BOX 14
FPO 09499-0014

10. SPONSOR/MONITOR'S ACRONYM(S)

11. SPONSOR/MONITOR'S REPORT NUMBER(S)
CSP 02-5077

12. DISTRIBUTION/AVAILABILITY STATEMENT

Approved for public release; distribution is unlimited.

13. SUPPLEMENTARY NOTES

14. ABSTRACT

The Final Proceedings for High Sensitivity Magnetometers 'Sensors and Applications', 4 November 2002 - 8 November 2002

Magnetic sensors designed to operate both at room temperature and at cryogenic temperatures. Applications of these sensors will also be addressed, including non-destructive evaluation of composite materials, magnetic anomaly detection, space magnetism, and geomagnetism.

15. SUBJECT TERMS
EOARD, Magnetic Resonance Spectroscopy, Quantum Well Devices

16. SECURITY CLASSIFICATION OF:			17. LIMITATION OF ABSTRACT	18. NUMBER OF PAGES	19a. NAME OF RESPONSIBLE PERSON
a. REPORT	b. ABSTRACT	c. THIS PAGE			David M. Burns, Lt Col, USAF
UNCLAS	UNCLAS	UNCLAS	UL	61	19b. TELEPHONE NUMBER *(Include area code)* +44 (0)20 7514 4955

Standard Form 298 (Rev. 8/98)
Prescribed by ANSI Std. Z39-18

609 047

We wish to thank the following for their contribution to the success of this conference:

Centre National de la Recherche Scientifique

European Office of Aerospace Research and Development,
Air force Office of Scientific Research, United States Air Force Research Laboratory

University of CAEN

Conseil Régional de Basse Normandie

SCIENTIFIC COMMITTEE

G. BARTINGTON, P. SEIDEL, P. RIPKA, J. RANSON, K. MOHRI,
D. DURET, A. FERT, D. PLACKO CH. DOLABDJIAN, D. ROBBES,
M. LAM CHOK SING, D. BLOYET, S. FLAMENT, H. GILLES

LOCAL ORGANIZING COMMITTEE

CH. DOLABDJIAN, D. ROBBES, M. LAM CHOK SING, H. GILLES, S. FLAMENT

Contact:

Pr. CH. DOLABDJIAN
GREYC (GROUPE DE RECHERCHE EN INFORMATIQUE, IMAGE ET INSTRUMENTATION DE CAEN)
6, BD DU MARELCHAL JUIN
F-14050 CAEN CEDEX

EMAIL: c.dolabdjian@greyc.ismra.fr
WEB: http://www.greyc.ismra.fr/EquipeInstru/cdolabdjian/index.html

Program (November 4-8, 2002)

Accommodation will be arranged for participants arriving on Sunday evening (after 18 h.) with dinner at 20H30-21H30

	Monday	Tuesday	Wednesday	Thursday	Friday
7h15-8h15					
8h30-9h10	*Late Arrival*	**Absolute magnetometers** J.M. Léger	**Magneto-optic** S. Flament	**Magnetic anomaly detection** Y. Bourez	**Metrological applications** F. Piquemal
9h10-9h50		**Induction sensors** A. Yashan	**μmagnetometer** F. Baudenbacher	**Geomagnetism** J. Rasson	**Active Shielding** H. Nowak
9h50-10h10		*Coffee break*	*Coffee break*	*Coffee break*	*Coffee break*
10h10-10h50		**Fluxgate Magnetometers** F. Primdahl	**Noise Reduction Technic** M. Lam Chok Sing	**Space Magnetometry** F. Primdahl	**Others Applications** A. Platil
10h50-11h30		**Hall sensor** V. Mosser	**Round table: Sensors**	**NDE: Surface defect detection**, A. Yashan	**Magnetic Microscopy** F. Baudenbacher
11h30-12h10	**Opening & Introduction,** C. Dolabdjian	**YIG magnetometer** P. Nikitin		**NDE: Buried defect detection**, M. Kreutzbruck	**Round table: Applications**
12h45-13h45					
14h00-14h40	**Magnetic Sensors Overview** P. Ripka	**SQUID** M. Schilling	*Departure: 13H00* *Sightseeing tour* *at M^t S^t Michel*	**MagnetoEncephalography** J. Vrba	*Departure: 13 H 15* *To* *Valognes Station* *Train to Paris: Departure: 14h19*
14h40-15h20		**Magnetoinductive sensors** L. Panina		**Magnetocardiography** M. Ter Brake	
15h20-16h00	**Sensors Specification** C. Dolabdjian	**Magnetoresistive sensors:** MR, GMR, CMR		**Others Biomagnetism Applications**, K. Enpuku	
16h00-16h20	*Coffee break*	*Coffee break*		*Coffee break*	
16h20-17h00	**Noise source rejection** J. Vrba	MR, GMR, CMR S. Tumanski		**Low field NMR imaging** J. Clarke	
17h00-17h40		**Poster presentation: Sensors**		**Poster presentation: Applications**	
17h40-18h00	*Presentation of GREYC laboratory* D. Robbes				
18h00-19h00	*Poster preparation*				
19h30-20h30	*Dinner*	*Dinner*	*Dinner(20H00-21H00)*	*Workshop Dinner*	
20h45		**Round table : EUROPEAN Project**	*Poster Preparation*		

CONTENTS

SENSORS

Magnetics sensors overview (P. Ripka)

Pavel Ripka
Czech Technical University
Technicka 2, 166 27 Praha 6, Czech Republic,
Email: ripka@feld.cvut.cz

The main types of magnetic sensors are:

1. Semiconductor sensors (mainly Hall)
2. Permalloy magnetoresistors (AMR, GMR)
3. Resonant magnetometers (Proton, Cesium, Overhauser)
4. SQUIDs (LTS + HTS)
5. Induction coils, rotating coils
6. Fluxgate
7. Optical (Fibre optic and thin-layer)
8. Other principles (MI, GMI, magnetoelastic, force, ...)

INDUSTRIAL SENSORS

Vast majority of produced magnetic field sensors are Hall devices and their main application is position sensing with help of permanent magnets. Hall sensors are cheap and they can be easily integrated with electronic circuits. However they will be gradually replaced by more sensitive ferromagnetic magnetoresistors: AMRs (anisotropic) and GMRs (giant) and in the future also SDT (spin-dependent tunneling) devices. These allow to use smaller or cheaper magnets and increase the sensing distance. Hall sensors are the only practical semiconductor magnetic field sensors. Semiconductor magnetoresistors, magnetodiodes and magnetotransistors are either outdated or exotic devices.
Magnetoinductive, magnetoimpedance (GMI), CMRs and magnetostrictive field sensors are unlikely to become widely used by industry because of their questionable stability and high price.

HIGH FIELD SENSORS

They include optical and force sensors. Magneto-optical sensors have an application potential in the measurement of large electrical currents ("optical transformers"). Also microfabricated force sensors can work linearly in very high fields, but have poor resolution in low fields.

SENSORS FOR MAGNETOMETERS

Magnetometers are produced in low volumes and the price of the sensor is not so critical. The most precise Earth's field magnetometers can detect sub-nanotesla variations. They combine absolute precision of resonant magnetometer with directional sensitivity of fluxgate sensors.

For sensor selection it is important to consider the following questions:

SCALAR VERSUS VECTORIAL

Scalar sensors measure the total value of the field, while vectorial sensors are directional. Scalar sensors are based on resonant principles and usually measure absolute value with large precision. Their main disadvantage is usually the sensor size and limited measuring range – they fail in zero field.

Magnetic field vector can be calculated from the readings of the scalar sensor if we add to it well defined precise field steps of changing directions. Also total field value can be calculated from reading of three orthogonal vectorial sensors. It is important to use instantaneous samples for this calculation to avoid dynamic error. But these indirect techniques bring additional errors.

LOW- OR ROOM-TEMPERATURE

SQUID sensors measure only small field changes. Their full-scale range is very limited and they are rarely used for direct measurements – they are usually configured as high-order gradiometers. Although SQUIDs are in principle fast, flux-locked magnetometers cannot follow fast field changes. While the most popular are the biomagnetic applications such as MEG, most of SQUID magnetometers are used to measure magnetic properties of small and/or magnetically weak samples. High-temperature SQUIDs which work in liquid nitrogen are noisy.

AC or DC

If induction coils do not move, they measure only AC fields. Most other magnetometers measure also DC field component. Some induction magnetometers use the search coil in current-output mode. This makes the sensitivity independent of frequency (in limited frequency range) and also can give low noise.

FERROMAGNETIC OR NOT

Ferromagnetic concentrators are sometimes used to increase the sensitivity of Hall sensors or magnetoresistors. For the same purpose some induction coils use ferromagnetic core. This technique can degrade the sensor linearity, but main danger is perming error caused by magnetic hysteresis. For proper operation the core or concentrators should be periodically demagnetized, which is rarely implemented in existing designs.
Fluxgate sensors are based on nonlinear properties of ferromagnetic material. The core is periodically saturated which should remove the perming – nevertheless only very expensive fluxgates reach the precision of absolute resonant sensors.

Many principles can be used for measurement of the magnetic field – but the selection of magnetic sensors for practical applications is very limited.

Magnetics Sensors Specifications (C. Dolabdjian)

Christophe Dolabdjian
Groupe de Recherche en Informatique, Image et Instrumentation de CAEN
6, Bd du maréchal Juin, F-14050 CAEN Cedex
email : c.dolabdjian@greyc.ismra.fr
http://www.greyc.ismra.fr/EquipeInstru/cdolabdjian/index.html

INTRODUCTION

Besides other well known sensors, magnetic sensors have specific peculiarities. They can be describes like classical electronic systems [1] and completed with their specific characteristics. In general, manufacturer's datasheet or researcher's scientific publications give some of them, but do not mention numerous others. The objective of this talk is to give an overview of the most important magnetic sensor characteristics so as to clarify sensors comparison and use.

CHARACTERISTICS

Table I resumes magnetic sensor characteristics in homogeneous or in inhomogeneous magnetic field detection with or without spatial filter configuration using gradiometric structure. In practice, all these absolute specifications should be given in the units of the measurement. Some of them, like sensitivity, should be referred to the sensor output information and the measuring conditions should be specified.

Homogeneous magnetic field	*Electromagnetic Compatibility*
Classical	- Electromagnetic compatibility (Electromagnetic perturbation sensitivity)
- Sensitivity (V/T, Hz/T, A/T)	
- Equivalent noise spectral density referred at the input, including the white noise level and the low frequency excess noise.	*"Real world" characteristics*
- Signal to Noise Ratio	- Main signal and noise characteristics of the sensor-operating environment
- Dynamic range	
- Bandwidth	*Industrial*
- Slew-rate	- Working temperature range…
- Linearity	- Power needed to operate the devices (Ex: with and without cryogenic refrigerator)
- Working type (Open Loop or Flux Locked Loop)…	- Portability
	- Price…
Static or Ultra Low frequencies	
- Long term stability and ageing	***Inhomogeneous response*** *(Ex: magnetic moment response versus a magnetic dipole)* - "When sensors could not be considered as a punctual sensor"
- Sensitivity parameters to temperature drifts and other external parameters inducing possible drifts	
- Hysteresis, Perming (offset after an important magnetic field perturbation)	- Evolution of the classical characteristic
- Field gradient sensitivity…	- Spatial resolution
	Gradiometer
Spatial response	
- Field Diagram (Ex: variable axis magnetic field response versus a homogeneous magnetic field)	- Evolution of the classical characteristic
- External size of sensor, packaging, minimal distance (source - sensors)	- Noise level rejection versus noise gradient
	- Spatial filter characteristic…

Table I: Main magnetic sensor characteristics

It is possible to classify these characteristics in six groups (classical characteristic [2], "real world" characteristic (open environment), static or ultra low frequencies characteristic [2], spatial response, ElectroMagnetic Compatibility and industrial characteristic) (see Table I) and complete them by some multi sensors parameters (see Table II).

MULTI SENSORS CHARACTERISTICS

Multi sensors evolution parameters
- Reproducibility - Integrability of the technology - Cross-talk…

Table II: Main magnetic multi-sensors characteristics

CALIBRATION

The main part of this characterization can be made with pre-calibrated Helmholtz coil pair. The disturbing field should be small; the ideal calibration coil is located, ideally, in a thermostated nonmagnetic house far from the sources of magnetic pollution. The noise measurement can be made in magnetic shielding or shielded room. The sensor's spatial resolution can be achieved with an equivalent magnetic moment as source.

OBJECTIVES APPLICATIONS

Table III resumes needed sensor performances or specifications versus magnetic sensor characteristics and environment.

Synthesis table: Application (Requested performances)	
- Sensitivity - Noise level - Optimal signal to noise ratio - Dynamic range - Bandwidth - Slew-rate - Linearity - Time of measurement (integration)	- Allowed offset variation - Amplitude of magnetic field perturbation - Field gradient level - Working temperature range - Accessibility - Electromagnetic Perturbation - Needed magnetic spatial resolution -…

Table III: Main needed sensor performances versus applications

In conclusion, sensor characteristics are numerous. Generally, only some or requested performances are given according to the main objective sensor application. Meanwhile, to clarify the sensors comparisons and use, it will be necessary to develop these characterizations and some new critera like Merit Figure [3] can be introduced.

REFERENCES

[1] Analysis and Design of Analog Integrated Circuits, Paul R. Gray, Robert G. Meyer. Third Edition. John Wiley and Sons, Inc. 1993. New York
[2] "Magnetic sensors and magnetometer", Editor : P.Ripka, Artech house, 2001 Artech HOUSE, INC, 685 Canton street, Norwood, MA 02062
[3] C. Dolabdjian, A. Qasimi, D. Bloyet, Physica C 368(2002), 80-84

Rejection of noise sources (J. Vrba)

Jiri Vrba
CTF Systems Inc., A subsidiary of VSM MedTech Ltd., Port Coquitlam, B.C., Canada

Superconducting quantum interference device (SQUID) based magnetometers are the most sensitive detectors of magnetic fields presently available. Their most important commercial application is to magnetoencephalography (MEG). Modern multi-channel MEG instruments typically have several hundred channels and the MEG alone is the largest consumer of the SQUID magnetic sensors with well over 12,000 SQUIDs installed to date. The MEG systems are usually operated within shielded rooms. But even within these shields a large residual environmental noise is present and deployment of highly efficient noise cancellation techniques is required. This presentation will concentrate on these noise reduction methods. First, construction of SQUID sensors will be briefly reviewed, followed by a discussion of practically achieved sensitivities. The SQUID sensitivity will be contrasted with the typical environmental noise magnitudes and answer to the question of "how much noise cancellation is necessary for MEG applications" will be suggested. Then various noise cancellation techniques will be discussed, including shielding, noise cancellation by primary sensors, reference based noise cancellation, active shielding, and noise cancellation by spatial filtering.

SQUID SENSORS AND NOISE

The SQUID sensors themselves are usually not directly suitable for detection of the required magnetic fields. For these reasons the SQUIDs are coupled to superconducting flux transformers, which consists of pickup coils, leads, and coupling coil; the pickup coils are designed for a good match to the measured fields. Because the flux transformer circuit is superconducting it does not contribute noise and its frequency response is flat from dc up to the maximum operating frequency. The pickup coils play an important role in noise cancellation and they can be configured to represent magnetometers, 1^{st}-order, or higher-order hardware gradiometers. The noise cancellation requirements, especially in unshielded environments, dictate stringent performance parameters on the SQUID sensors and electronics: large dynamic range, high slew rate, good linearity and good matching between SQUID channels (similar requirements are also important for successful analysis of MEG signals by array signal processing methods).

Noise acting on an MEG detection channels can be roughly divided into three components: (1) Random noise which is due to SQUID sensors or their electronics. This noise is uncorrelated among channels; (2) Environmental noise caused by moving magnetic objects or electric currents, e.g., cars, elevators, power lines, electric machinery, etc. This noise is usually caused by distant sources; and (3) Near-field noise due to electrophysiological activity of the human body, e.g., muscles, heart, eyes, parts of the brain which are of no interest, etc. The environmental and body generated noise are correlated among the channels. The SQUID sensor sensitivity (or the random noise in part 1) is in the range of femto-Tesla (fT), while the low frequency environmental noise magnitude within shielded rooms can be as high as 10 nT and about 1 □T unshielded. This represents dynamic range of up to about 10^8 and also indicates the degree by which the noise should be reduced.

NOISE CANCELLATION

Noise cancellation is usually accomplished by a combination of complementary hardware and synthetic methods including shielding, suitable design of pickup coil geometry, reference based methods (gradiometers and adaptive), active shielding, and by spatial filtering.

Shielding is the simplest approach to the noise reduction. The present biomagnetic systems are typically operated in shielded rooms with modest low frequency attenuation of less than 100 and attenuation increasing at higher frequencies. In addition to shielding, optimization of the flux transformer pickup coil geometry is the next obvious hardware method for the noise reduction. Since the signal-to-noise ratio (SNR) is the most important parameter which determines the MEG ability to detect brain sources, the pickup coils are designed to optimize the SNR by maximizing the brain signal magnitude while minimizing the detected environmental noise. The SNR optimization leads to gradiometer pickup coil configurations with relatively short baselines (3 to 8 cm). Active shielding is the third hardware method considered in this presentation. It will be shown that the active shielding with practically dimensioned coils contributes large gradients and is not suitable for MEG systems which employ gradiometers.

The MEG sensor array typically consists of primary sensors and references. The primary sensors are exposed to the brain fields and the references are used for noise cancellation. The primary sensors are usually magnetometers or 1^{st}-order hardware gradiometers. It is also possible to construct higher-order hardware gradiometers, however, they are bulky, laborious to produce, and inaccurate. For these reasons synthetic gradiometers were developed. Synthetic gradiometers are generated by subtracting a linear combination of the reference outputs from the primary sensor outputs. The references can also be utilized to synthesize different systems than gradiometers. For example, the subtraction coefficients can be determined to minimize noise observed during a "training" period. These adaptive systems can exhibit better noise cancellation than the gradiometers, however, while the gradiometer coefficients are universal and independent of the noise character or the dewar orientation, the adaptive coefficients depend on both and may have to be re-determined frequently.

A powerful noise cancellation can be achieved by spatial methods. The simplest such method is signal space projection (SSP). The measurement is represented by a vector in a multidimensional signal space, where the number of dimensions equals to the number of channels. Vectors corresponding to the noise are estimated (e.g., by measuring noise in the absence of a subject) and the measurement is then projected to a subspace orthogonal to the noise subspace. Such projection eliminates the noise while it preserves the signal, provided that the signal is not entirely in the noise subspace. A more selective method is to use beamformers. Beamformer is a spatial filter corresponding to a selected location and constructed as a linear combination of the measurements. The weights of this linear combination are determined by minimizing the filter power subject to the condition of unity gain from the investigated location. The beamformers isolate signal from the selected location by projecting sensitivity nulls to the vicinity of the interfering sources. The beamformers are more selective than the SSP and efficiently eliminate the far-field environmental and near-field body generated interference.

The existing MEG systems utilize diverse noise cancellation methods. Combination of these methods was shown to reduce noise by up to more than seven orders of magnitude to the levels that are adequate for high quality detection of the brain signals. Some methods, especially the spatial filtering methods, are used both for noise cancellation and for interpretation of MEG signals.

Absolute magnetometers (J.M. Léger)

J.M. Léger

Inductive sensors: High-spatially resolved material characterisation with Barkhausen noise and Eddy current MIcroscope – BEMI (A.Yashan)

Andriy Yashan
Fraunhofer Institute for Non-destructive Testing, IZFP, University Building 37, 66123 Saarbruecken, Germany
Email: yashan@izfp.fhg.de

Inductive sensors are one of the oldest types of magnetic field sensors and stay the most usual sensor type for the electromagnetic methods of non-destructive testing of materials. The following paper is dedicated to material characterisation with eddy current (EC) technique and Barkhausen noise measurement using a small induction sensor.

In the EC technique, the excitation coil of the EC transducer is driven by a small alternating current. The variables are the operating frequency (EC frequency) to influence the sensed volume depth by the skin effect and the sensor design. The electromagnetic field caused by the excitation current is affected by an electrically conductive and / or ferromagnetic specimen under test. All microstructure changes of specimen influencing the electrical conductivity and / or the magnetic permeability as well as geometrical discontinuities (defects) can be detected by measuring the voltage induced in the detection coil of the EC transducer.

In magnetic Barkhausen noise measurement, electrical pulses are induced in an inductive sensor by tracing the hysteresis curve (magnetisation curve) of a ferromagnetic specimen. Frequency spectra of the detected pulses are in the range between 0 Hz (dc) and 2-3 MHz.

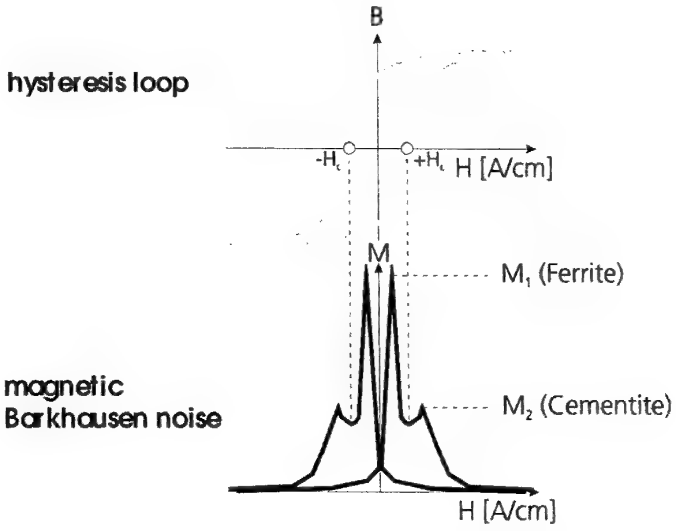

Figure 1: Barkhausen noise profile curve of a pearlitic microstructure state

One common signal processing technique after receiving and amplification of the voltage pulses is band-pass filtering, followed by rectifying and low-pass filtering. As function of the applied field (x, y-presentation) profile curves like that shown in Figure 1 can be documented. Single and multiple peaks are detected, depending on the number and on the noise activity of different involved magnetic phases in the

material. Therefore, different peak maxima, peak separations and the peak width can be derived as characteristic parameters. In Figure 1 the relationship to coercivity is also indicated.

Using the **B**arkhausen Noise and **E**ddy Current **Mi**croscope (BEMI) developed by IZFP Saarbruecken enables fast measurement of magnetic properties with the spatial resolution down to 10 μm [1]. The used induction sensor is a coil system with magnetic circuit consisting of a small yoke with a very small air gap of approx. 0.1 μm. The computer-controlled positioning unit of the BEMI allows the sensor to find selected measuring points or to produce measuring scans. The integrated three-axis positioning system has a positioning accuracy of < 1 μm for all directions.

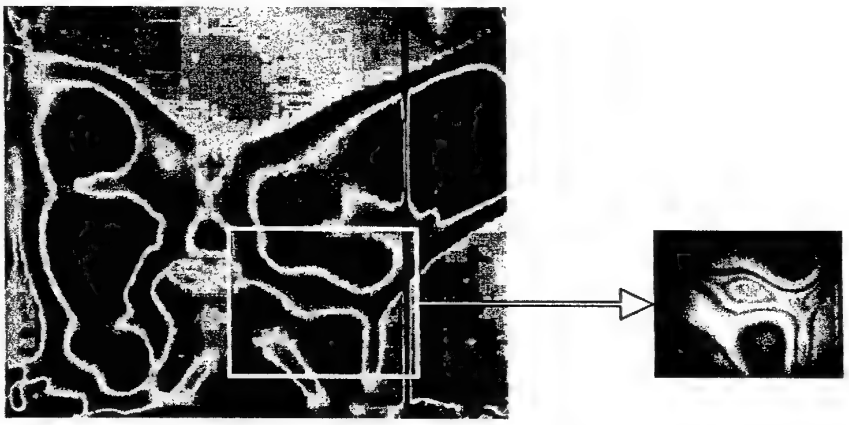

Figure 2: Eddy current microscopy image of thickness variation of a thin film (left) and the optical image as a reference (right).

Figure 2 (left) shows the result of EC measurement using BEMI obtained on a thin polyimide film with a depth of 400 nm on a ferrite body. The size of the scanned area is 10*8 mm^2. The information in the indicated frame is in accordance with the optical microscope image (Figure 2 right) that shows Newton rings due to the variation of the film thickness.

The Barkhausen noise measurement using BEMI enables fast imaging with high local resolution of residual stress distributions in specimens [2].

REFERENCES

[1] J. Bender, "Barkhausen Noise and Eddy Current Microscopy (BEMI): Microscope Configuration, Probes and Imaging Characteristics"; in Review of Progress in Quantitative Nondestructive Evaluation; D.O. Thompson, D.E. Chimenti (eds.) Plenum Press New York (1997) 16B, 2121-2128

[2] I. Altpeter, G. Dobmann, N. Meyendorf, S. Fassbender, J. Hoffmann, W. Nichtl-Pecher, J.G. Johnson, "Detection of Residual Stresses and Nodular Growth in Thin Ferromagnetic Layers with Barkhausen and Acoustic Microscopy", in Nondestructive Characterization of Materials VIII (1998), 677-682; International Symposium on Nondestructive Characterization of Materials; 8, June 1997, Boulder, Colorado

Fluxgate Magnetometers (F. Primdahl)

Fritz Primdahl
Danish Space Research Institute and Measurement & Instrumentation, Oersted·DTU, Technical University of Denmark, Building 327, Elektrovej, DK-2800 Kgs. Lyngby, Denmark. fpr@oersted.dtu.dk 10/10 2002FP

INTRODUCTION

The fluxgate magnetic field transducer is basically a small transformer with a ferromagnetic core, which is sensitive to external dc and low frequency ac magnetic fields. The core is periodically saturated by a large primary ac excitation current (typically in the range 50Hz to 50kHz). The secondary coil picks up a distorted induced signal, where certain characteristic parts of the distortion carries the information about the external B-field coupled to the core.

The first description of the fluxgate used to measure magnetic field fluctuations is believed to be by Aschenbrenner and Goubau (1936), who used a ring-core sensor as early as in 1928 [Geyger, 1958]. The need for magnetometry for surveys and geological exploration spurred the development of sensors and electronics during the 1940'ies and 1950'ies [see e.g. the review by Primdahl, 1979], and following many sounding rocket launches, the first magnetometer (a fluxgate) was launched into Earth's orbit onboard Sputnik-3 in May 1958 [Dolginov, 1998].

Following a brief summary of the range of performance parameters, the remaining part of this paper discusses the sub-systems of a high-performance vector magnetometer and touches upon the instrument calibration procedures.

PERFORMANCES PARAMETER

The ideal ferromagnetic material has a remarkable symmetry for magnetization by external fields in the sense that a change of sign of the external field produces exactly the same magnitude of magnetization in the material but in the opposite direction. This property is fundamental for the intrinsic solid-state physics of the magnetic materials. The balance is demonstrated by the fact that the amorphous magnetic material VITROVAC 6025 [Vacuumschmeltze, 2002] has a saturation magnetization ($\mu_o M$) equal to ~ 0.5T. The zero-level offset is typically about 5 nT with a stability over time and temperature of fluxgate sensors made of this material of ~0.5nT [Olsen *et al.*, 2002], i.e. a symmetry of the order of 10^{-8} and a reproducibility of the order of 10^{-9} of the magnetization process.

The output response of a well-designed fluxgate sensor is (for modest fields) linear [Acuna and Ness, 1975] and proportional to the cosine of the angle between the external field vector and a characteristic magnetic axis of the sensor [Acuna and Pellerin, 1969]. An orthogonal combination of three fluxgate sensors then measures the vector components of the external magnetic field. The equivalent noise power spectral density of a high-quality fluxgate sensor follows the 1/f-law at ultra-low frequencies, and is reported to be well below $20pT_{rms}$ in a frequency band from 0.01Hz – 10Hz [Nielsen *et al.*, 1995 & 1997, Primdahl, 1979]. Larger ring-core sensors have lower noise, and for 25mm diameter cores the noise power spectral densities are reported as low as $2.8pT/Hz^{1/2}$ at 1Hz (stress-annealed V6025) [Peter Brauer, private communication, 2000] and $3.8pT/Hz^{1/2}$ at 1Hz (annealed crystalline permalloy) [Ripka, 2000, p. 107]. The Voyager magnetometers achieved an RMS noise in a "dc-1Hz" bandwidth of 1pT in the quietest environment in the solar system – the Jovian tail [M.H. Acuña, private communication, 2002]. The frequency response may approach the excitation frequency. However, at about 1kHz the sensitivity of an induction coil of comparable dimensions crosses that of the fluxgate [Ripka, 2000]. Ground-based Magnetic Observatory magnetometers have typically 1Hz response frequency [DMI], many satellite magnetometers have sampling rates in the range from 10 to 100 samples/second or higher, and sounding

rocket instruments may have responses in the kHz-range [Pedersen *et al.*, 1999; Ripka *et al*, 1995]. A high-performance space magnetometer may consume less than 400mW and weigh less than 600g including sensor and cable.

THE FLUXGATE SENSOR

The saturation of the core causes symmetric distortion (odd harmonics) of the primary excitation waveform at the output, whereas a superposed dc magnetic field upsets the magnetization symmetry and causes an asymmetric (even harmonics) output to appear. For small fields (below ~1μT) this is near proportional to the external field component along the sensor magnetic axis. Viewed in the time domain, the core looses its permeability for the external field whenever saturated; the external flux is then periodically excluded from the secondary coil, and this change induces the field-dependent signal. This gave rise to the US-name "Flux-Gate", originally coined by Bendix Aircraft Corporation.

Many sensor designs have been devised and optimized for suppressing the symmetric saturation-distorted signal and enhancing the external-field-dependent asymmetric signal, the double-rod sensor and the ring-core being the most common [Primdahl, 1979; Ripka, 2000]. A feed-through to the output of the excitation signal exists even in the best-balanced sensors. This means that the even-harmonics content in the excitation current should be kept correspondingly low, and that the field-dependent even-harmonics sub-nT signal must be detected in a background of 0.5 - 5μT over-coupled odd-harmonics.

For low-power excitation of the ring-core fluxgate sensor a parametric resonance primary drive circuit is widely used [Berkman *et al.*, 1972; Acuna, 1974]. By tuning the secondary coil to (or near) one of the even harmonics, the field-dependent output signal may be enhanced or amplified by parametric resonance in the output circuit [Ripka and Primdahl, 2000].

The B-field inside the sensor core material is related to the external dc field B_o by the core material susceptibility χ and the geometry-dependent demagnetizing factor D: $B = \{(1+\chi)/(1+D\chi)\}B_o$. Double-rod sensors typically have $D \approx 1\text{-}3\times10^{-4}$ and ring-cores have $D \approx 0.4\text{-}4\times10^{-3}$ [Primdahl *et al.*, 2002b].

SIGNAL PROCESSING

The sensor secondary coil is coupled unloaded to the high-impedance input of the signal-conditioning amplifier, or short-circuited by the low-impedance input of a current-feedback operational amplifier. The coupling may be broadband or band-limited by tuning the sensor secondary [see Ripka and Primdahl, 2000, and references therein]. In the frequency domain one of the excitation even harmonics (usually the second) in the unloaded/tuned sensor signal is filtered out and synchronously detected under phase control of the excitation signal. The detector output is a double-rectified sine wave whose dc component is proportional to the external magnetic field component along the sensor magnetic axis. In the time-domain the broadband current impulses from the short-circuited sensor are synchronously gated under timing control of the excitation generator circuit. Again, the dc content of the impulse series output is proportional the external field along the sensor [Primdahl *et al.*, 1989].

Rather than using the dc content of the synchronously detected sensor signal directly as the measure of the magnetic field component, a feedback loop is established by connecting the detector output through an integrator and via a voltage-to-current converter (often just a large resistor) to the secondary coil or to a separate feedback coil [Primdahl and Jensen, 1984]. The feedback current establishes a balancing magnetic field that near-cancels the external field along the sensor axis. Only a very small residual field remains, just sufficient to sustain the feedback current via the large loop gain. This current is then a highly linear replica of the axial external field, and by measuring the current directly only the coil linear temperature expansion coefficient needs to be compensated for.

Analogue signal processing followed by an output analogue-to-digital-converter (ADC) is still dominantly used, but instruments implementing the filtering, detection, integration, feedback generation and the telemetry interface as algorithms in a digital signal processor were successfully flown onboard

several sounding rockets and on the Swedish micro-satellite Astrid-2 [Merayo *et al.*, 2002; Pedersen *et al.*, 1999].

CALIBRATION

The calibration matrix and offset vector define the intrinsic sensor coordinate axes. The x-axis is taken along the first physical magnetic axis. The y-axis is perpendicular to the x-axis and taken in the plane extended by the first and the second magnetic axes. The z-axis then completes the right-handed orthogonal coordinate system. The calibration of a tri-axial fluxgate sensor consists first of the determination of the parameters of the intrinsic reference system, i.e. the scale values $S_{1,2,3}$, the offsets $O_{1,2,3}$ and the inter-axes deviation angles from orthogonality $v_{1,2,3}$ [Risbo and Olsen, 1996; Olsen *et al.* 2002]. Next, the directions of (at least) two externally accessible reference axes (optical mirror normals or mechanical surfaces) shall be determined in the intrinsic sensor reference system. The optical/mechanical reference axes constitute the link to any external coordinate system, e.g. geodetic or satellite coordinates, etc.

The nine calibration parameters above constitute a linear and invertible model (in B), and the determination may be done in a calibrated test coil system using the "Thin Shell Method" [Risbo and Olsen, 1996; Risbo *et al.* 2002]. Alternatively, the intrinsic parameters may be determined by rotating the fluxgate sensor in the Earth's field (monitored by an absolute scalar resonance magnetometer) by the "Scalar Calibration Method" [Merayo *et al.* 2000] The link to the SI-unit for magnetic field is established by the calibration of the test coil system or by direct comparison with the readings of an absolute scalar magnetometer. Besides the calibration parameters, also the temperature coefficients of the parameters shall be determined over the anticipated temperature range.

Low-level non-linearities exist in fluxgate magnetometers. The most common types are in-axis non-linearities caused by the electronics and the ADC, and for ring-cores, in addition, the off-axis Transverse Field Effect (TFE) non-linearity. The in-axis effects can be modeled in the laboratory by polynomials and corrected for before the linear calibration parameters are determined. The TFE may also be modeled by an expression containing the transverse field and corrected for prior to matching the linear model parameters [Brauer *et al.* 2002].

The externally accessible axes' directions relative to the intrinsic sensor coordinate system may be determined by rotating the calibrated sensor about these axes in a test coil facility or in the monitored Earth's magnetic field [Primdahl *et al.* 2002a].

REFERENCES

Acuna, M. H., Fluxgate Magnetometers for Outer Planets Exploration, **IEEE Trans. Mag., 10**, 519-523, 1974 .

Acuna, Mario H., and Charles J. Pellerin, A Miniature Two-Axis Fluxgate Magnetometer, **IEEE Trans. Geosci. Electron., GE-7**, 252-260, 1969.

Acuna, Mario H. and Norman F. Ness, The Pioneer XI High Field Fluxgate Magnetometer, **Space Science Instrumentation, 1**, 177-188, 1975.

Aschenbrenner, Hans und Georg Goubau, Eine Anordnung zur Registrierung rascher magnetischer Störungen (An Arrangement for Recording of Fast Magnetic Disturbances), **Hochfrequenztechnik und Electroakustik** (Jahrbuch der drahtlosen Telegraphie und Telephonie), Leipzig, Germany, **Vol. 47, no 6**, 177-181, 1936, (in German).

Berkman, R. Ja., V.L. Bondaruk and V.M. Fedotov, Ferroresonance Mode of Excitation of Magnetic Modulators and Fluxgate Sensors, **Geofiziczeskaya Apparatura**, **50**, 20-28, 1972 (in Russian).

Brauer, P., T. Risbo, J.M.G. Merayo and F. Primdahl, New Method for Calibrating Non-Linear Ring-Core Fluxgate Magnetometers, **Sensors and Actuators A, 82,** (submitted), 2002.

DMI, Fluxgate Magnetometer FGE, Danish Meteorological Institute, Solar-Terrestrial Physics Division, Lyngbyvej 100, DK-2100 Copenhagen Oe, Denmark, Telephone: (+45) 39 15 75 00.

Dolginov, Sh. Sh., The First Magnetometer In Space, in G. Haerendel *et al*. (eds.), *40 Years of COSPAR,* **ESA Publications Division**, ESTEC: Noordwijk, The Netherlands, 55-63, 1998.

Geyger, William A., Self-Balancing Fluxgate Magnetometer, **AIEE Trans., Part 1, Comm. & Electron., 77**, 213-216, 1958.

Merayo, José M.G., Peter Brauer, Fritz Primdahl, Peter S. Jørgensen, Torben Risbo, and Joe Cain, The Spinning Astrid-2 Satellite Used for Modeling the Earth's Magnetic Field, **IEEE Trans. Geoscience & Remote Sensing, 40**, 898-909, 2002.

Merayo, J.M.G, P. Brauer, F. Primdahl, J.R. Petersen and O.V. Nielsen, Scalar Calibration of Vector Magnetometers, Meas. Sci. Technol., 11, 120-132, 2000.

Nielsen, O.V., J.R. Petersen, F. Primdahl, P. Brauer, B. Hernando, A. Fernandez, J.M.G. Merayo, and P. Ripka, Development, Construction and Analysis of the "ØRSTED" Fluxgate Magnetometer, **Meas. Sci. Technol., 6**, 1099-1115, 1995.

Nielsen, O.V., P. Brauer, F. Primdahl, T. Risbo, J.L. Jørgensen, C. Boe, C. Deyerle and S. Bauereisen, A High-precision Triaxial Fluxgate Sensor for Space Applications: Layout and Choice of Materials, **Sensors and Actuators A, 59**, 168-176, 1997.

Olsen, N., L. Tøffner-Clausen, T. J. Sabaka, P. Brauer, J.M.G. Merayo, J.L. Jørgensen, J.-M. Léger, O.V. Nielsen, F. Primdahl and T. Risbo, Calibration of the Oersted Magnetometer, **Earth, Planets and Space**, (submitted), 2002.

Pedersen, Erik B., Fritz Primdahl, Jan R. Petersen, J.M.G. Merayo, Peter Brauer and O.V. Nielsen, Digital Fluxgate Magnetometer for the Astrid-2 Satellite, **Meas. Sci. Technol., 10**, N124-N129, 1999.

Primdahl, F., P. Brauer, J.M.G. Merayo, J.R. Petersen and T. Risbo, Determining the Direction of a Geometrical/Optical Reference Axis in the Coordinate System of a Tri-Axial magnetometer Sensor, **Meas. Sci. Technol.**, (submitted), 2002a.

Primdahl, F., Peter Brauer, José M.G. Merayo and Otto V. Nielsen, The Fluxgate Ring-Core Internal Field, **Meas. Sci. Technol., 13**, 1248-1258, 2002b.

Primdahl, F., J.R. Petersen, C. Olin and K. Harbo Andersen, The Short-Circuited Fluxgate Output Current, **J. Phys. E.: Sci. Instrum., 22**, 349-354, 1989.

Primdahl, F., and P. Anker Jensen, Compact Spherical Coil for Fluxgate Magnetometer Vector Feedback, **J. Phys. E: Sci. Instrum., 15**, 221-6, 1982.

Primdahl, F., The Fluxgate Magnetometer, J. Phys. E: Sci. Instrum., 12, 241-53, 1979. (Review).

Ripka, P. and F. Primdahl, Tuned Current-Output Fluxgate, **Sensors and Actuators A, 82**, 161-165, 2000.

Ripka, P., Induction Sensors and Fluxgate Sensors, in: Pavel Ripka (ed.), "**Magnetic Sensors and Magnetometers**", **Ch. 2 and 3**, 47-128, ARTECH HOUSE INC., Norwood, Massachusetts 02026, USA, December, 2000.

Ripka, Pavel, F. Primdahl, O.V. Nielsen, J.R. Petersen and A. Ranta, A.C. Magnetic-Field Measurement Using the Fluxgate, **Sensors and Actuators A, 46-47**, 307-311, 1995.

Risbo, T., P. Brauer, J.M.G. Merayo, O.V. Nielsen, J.R. Petersen, F. Primdahl and N. Olsen, Ørsted Calibration Mission: The Thin Shell Method and the Spherical Harmonics Analysis, **Meas. Sci. Technol.**, (submitted), 2002.

Risbo, Torben and Nils Olsen, Attitude Intercalibration of the Star Imager and the Spherical Compact sensor Magnetometer for the Ørsted Geomagnetic Satellite Mission, **Proceedings of the SPIE – The International Society for Optical Engineering, 2810**, 230-238, 1996.

Vacuumschmeltze GmbH & Co. KG, 2002, <**http://www.vacuumschmelze.de/** >

Sensors & Use – Hall Effect Sensors (V. Mosser)

PHYSICAL PRINCIPLE

A Hall sensor is usually a 4-terminal cross-shaped semiconductor devices (Fig. 1). The Hall effect is based on the Lorentz force exerted by a magnetic induction on the conduction electrons. In a basic configuration, a biasing current is sent through 2 opposite legs, whereas the Hall voltage: is measured at the two other terminals (Fig. 2):

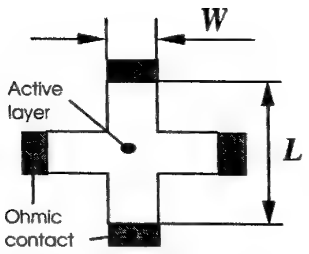

Figure 1: Schematic of a Hall sensor

$$V_H = K_H I\ B$$

The Hall cross-sensitivity K_H is related to the electron sheet density n_s by:

$$K_H = 1/en_s$$

Other key parameters are the electron mobility μ_n and the resulting square resistance $R_{sq} = 1/en_s\mu_n$. For a sensor with fourfold symmetry, the output impedance R_{out} is about the square resistance R_{sq} times the aspect ratio L/W (see Fig. 2). The aspect ratio L/W should be made ≥ 4. in order to avoid a shorting of the Hall voltage by contacts or magnetoresistance effects. Neither the magnetic sensitivity nor the square resistance or input resistance depend on the sensor size.

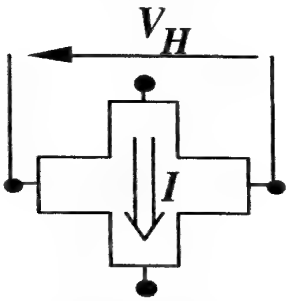

Figure 2: Biasing of a Hall sensor

Low cost/low performance Hall devices were traditionally made using a thin (μm) sheet of low doped n-type material on p-type or semi-insulating material.
Hall sensors using 2-dimensional conduction in quantum wells (QW) made of heterostructures of III-V semiconductors have emerged in the 90's as the most suitable solution for metrological applications.
A number of combinations fabricated on GaAs or InP substrates, all relying on modern epitaxy methods such as MBE or MOCVD, have been proposed in the literature. We have developed sensors based on the AlGaAs/InGaAs/GaAs system, because of its industrial availability, its low cost and its good performances in terms of stability.
These sensors are representative of the state-of-the-art. In the following, they will be used in most occasions as example sensors when numerical values are needed. Characteristic parameters of the heterostructure are $n_s = 8.7\times10^{11}$ cm^{-2}, $\mu_n = 7400$ cm^{2}V^{-1}s^{-1} and $K_H = 740$ V/AT $= 740\ \Omega$/T. Various different sizes have been investigated.
Others teams are developing others systems based on the InAlAs/InGaAs/InP family, because of the still higher electron mobility, but material properties are less well controlled.

Silicon based sensors may have an interest for some applications because they allow the integration of processing electronics, and/or the fabrication of large arrays of Hall sensors. However, their metrological performances in terms of mobility, sensitivity, stability, are much poorer.

In terms of measurement capabilities, the Hall effect constitutes a robust, non-intrusive, absolute measurement of a vector component of the flux density B_z. It is intrinsically a bridge measurement of a non-reciprocal effect. The combination of these two characteristics allows:
- the suppression of the common mode signal

- the possibility of the suppression of any offset voltage
- the possibility of suppression of any low-frequency noise originating in conductivity fluctuation.
- Moreover, its spatial resolution is roughly the size of the crossing region of the Hall cross. Some refinements allow extending the resolution of Hall measurement under the nT/√Hz region.
- In homogeneous magnetic field

Sensitivity

According to Eq. 1, the absolute magnetic sensitivity is proportional to the biasing current. Unfortunately, the bias current cannot be increased at will.

(i) An absolute limitation of the Hall sensitivity is provided by the saturation drift velocity v_{dsat} of the electrons. For all usual semiconductors, the saturation velocity v_{dsat} is in the 10^5 m/s range. The resulting current density $j_{S\,max}$ is in the 100 μA/μm range. This yields for the maximum sensitivity:

$$G_{H_{max}} = K_H\, I_{max} = K_H\, j_{max}\, W = v_{d_{sat}} W$$

For a jumbo sized Hall sensor with W = 100 μm, one gets an absolute sensitivity G_{Hmax} = 10 V/T, whereas for a 1 μm-sized Hall sensor the sensitivity will be G_{Hmax} = 0.1 V/T.

(ii) Practically, another limitation is likely to appear before the onset of drift velocity saturation, which is the self-heating due to the Joule effect.

The allowable current depends on many parameters such as the size of the active layer, the substrate material, whether the substrate is thinned or not, the type of mounting or packaging, whether the measurement is pulsed or continuous, the operating temperature and how much the temperature inside the active layer is allowed to increase.

Practically, for a given type of structure, the self-heating is approximately inversely proportional to the size of the active layer. It was found that for Hall sensors located on a thick (600 μm) GaAs substrate in a standard SOT plastic package, the sheet current density corresponding to a temperature increase ΔT=+1°C is about j_{max} = 10 μA/μm at room temperature, leading to a magnetic gain $G_H \approx 1$ V/T for W = 100 μm.

Equivalent noise spectral density

The noise at the Hall output is the sum of the thermal white noise, and the low frequency excess noise due to the fluctuation of the resistivity (or conductivity) of the active area:

$$S_{V_H} = 4\ kT\ R_{out} + S_{V_H}^{LF} \qquad \text{with} \quad S_{V_H}^{LF} = S_\rho \cdot I^2 \cdot \iint \left(\frac{\mathbf{j} \cdot \tilde{\mathbf{j}}}{I^2} \right)^2 ds$$

Several methods exist in order to get rid of the LF noise effects.

- The spinning current method, based on the non-reciprocity of the Hall effect, rejects the LF noises to high-frequency regions where it does not bother.
- The cross-correlation method, which makes use of two Hall sensors located in close vicinity, or even on top of each other.
- The modulation of the bias current, useful e.g. when measuring a small alternative low-frequency magnetic induction
- The concentration of the flux lines by soft ferromagnetic concentrators
- The combination of any of these methods.

In definitive, the real noise limitation is provided by the thermal noise: $S_{V_H} = 4\ kT\ R_{out}$, which amounts to a few nV/√Hz at room temperature, for R_{out} = 1000 to 4000 Ω. Depending on the mechanism limiting the bias current (cf. above), the noise spectral density can be expressed as:

$$S_B^{1/2} = \sqrt{\frac{4kT}{en_s\mu_n}} \Big/ v_{d\,sat} W \qquad \text{or} \qquad S_B^{1/2} = \sqrt{4kT\,\frac{en_s}{\mu_n}} \Big/ j_{s\,max} W$$

Best noise values for bare sensors are in the nT/√Hz range at room temperature and in the 100 pT/√Hz range at liquid nitrogen temperature.

Dynamic range

In a heterostructure based QW, the Hall sensitivity do not change in the nT-10 T range. E.g. in our example sensors, the relative change in sensitivity between 0.1 T and 20 T amounts to less than 2×10^{-3}.

Bandwidth and slew-rate

The intrinsic response time of the Hall effect is in the ps range. However, the Hall signal is delivered to the external world through resistive output legs. For any change of the Hall voltage, a transient current has to charge a capacitor whose capacitance is the sum of the input capacitance of the pre-amplifier and any stray capacitance.

Obviously the cut-off frequency directly depends on the charge capacitance. In our example sensor, each leg has a resistance of 1500Ω at room temperature. A 1 pF capacitance yields an 100 MHz cut-off. Some authors claim a cut-off frequency up to 1 GHz.

Linearity

QW based Hall sensors are perfectly linear in a very broad range in most operating conditions, cf. above.

The onset of the Quantum Hall Effect under liquid helium temperature at high induction value (B>0.5 T) destroys the linearity.

Thin layer based sensors, however, exhibit magnetoresistance effects and a poor linearity.

Open Loop / Flux Locked Loop

Open loop is often preferred when using high-quality devices. Some industrial applications are still using lower quality Hall sensors with secondary coils ensuring zero magnetic induction.

Long term stability and aging depend very much on the choice of the materials and on the process.

In our example sensors, accelerated aging studies showed no noticeable drift after 3000 h at 300°C, a lifetime in excess of 10^{11} hours was extrapolated. Packaged devices passed successfully a set of MIL-STD 202 tests (Dry Heat, Wet Heat and Rapid Thermal Variations).

- Sensitivity parameters to temperature drifts and other external parameters inducing possible drifts

The sensitivity to temperature depends on the heterostructure parameters (composition, doping, thickness of the different layer). Our example sensors show no thermal drift in the 4 K–130 K range, and a slight sensitivity decrease amounting to –140 ppm/°C in the –100°C/+180°C temperature range.

Perming (offset with an important magnetic field perturbation)

No such effect, due to the invariance of the sensitivity over a broad range of magnetic field.

Field gradient sensitivity

The Hall sensor is sensitive to the mean value of the induction B_Z over the crossing region of the Hall cross. For a given application, the size of the active layer should be chosen according to the required spatial resolution.

Working temperature range

Most heterostructure based sensors work down to liquid helium temperature or lower. Some heterostructure based sensors have been shown to work up to 200°C/500 K. Hall sensors based on silicon carbide SiC or nitrides (AlGaN/GaN) were reported in the literature showing operation over 600°C.

- External size of sensor and packaging

Chips with a discrete Hall sensor can be made as small as 500 μm×500 μm. For lower dimensions the handling becomes more difficult. The substrate thickness can be easily ground down to 150 μm.

Chips may be mounted bare on an epoxy or ceramic board. They may also be packaged in any plastic small outline package with typical dimensions as small as (L=2 mm,W=1 mm, t=0.9 mm).

- Field Diagram (Ex: variable axis magnetic field response versus a homogeneous magnetic field)

Heterostructure based QW devices are sensitive only to the vector component B_Z orthogonal to the active channel. The relative sensitivity to the in-plane B components is less than 10^{-3}, its experimental determination is limited only by the accuracy of the angle between B and the plane of the active layer.

- Electromagnetic compatibility (Electromagnetic perturbation sensitivity)

The derivative of the flux through the output circuit of the Hall sensor adds a contribution to the output signal: $V_{out} = V_H + V_{ind}$ with $V_{ind} = -d\Phi/dt$

The equivalent area of the output circuitry should thus be made as small as possible.

- Main signal and noise characteristics of the sensor-operating environment

- **Power** needed to operate the devices

For a jumbo (W=100 μm) sensor under1 mA biasing, the dissipated power typically amounts to a few mW.

For a small (W=2 μm) sensor under 40 μA biasing, the dissipated power amounts to 10 μW.

- **Minimal distance**

For a plastic packaged sensor, the minimal distance to the source is typically 200 to 300 μm. For a bare sensor without encapsulation, the minimal distance can be as small as 1000 Å (unpassivated sensor) or 4000 Å (passivated sensor). A protective resist layer with typical thickness a few μm can be deposited on top of the sensor.

- **Portability**

- **Price**

Depends very much on the choice of the materials, and on the quantity. Whereas basic Hall sensors are produced in billions units with a unit price lower than 10 cts, some III-V based QW Hall sensors are produced in quantities of millions units with a cost less than 1€ or 1$ per mm^2.

Special developments requiring foundry process and design of lithography masks may be envisioned with a budget of 100 k€.

Inhomogeneous response (Ex : magnetic moment response versus a magnetic dipole)

- **Spatial resolution**

The spatial resolution is roughly the size of the crossing region of the Hall cross, i.e. the active layer width W. Sensors with width comprised between 200 μm and 0.5 μm have been reported.

- **Merit figure**

to be discussed

Multi sensors evolution parameters

- **Reproducibility**

Due to the excellent homogeneity of MBE or MOCVD epitaxial materials, uniformity of characteristics across a wafer or among wafers from the same batch is within a few percent. The same figures are achievable through a well mastered industrial process.

- **Cross-talk**

The biasing current in the 100 μA – 1 mA range from a nearby sensor may induce a parasitic induction, which is however less than 1 nT at a distance of 20 μm.

- **Integration**

Several implementations of III-V based Hall sensors arrays with a pitch between 4 μm and 200 μm exist in the literature. Although none of them make use of on-chip multiplexing, this should be achievable at the cost of moderate efforts.

- **Gradiometer**

1D or 2D gradiometers can be easily implemented using the Hall effect, either implementing several Hall crosses on a single chip, or using 6 contact or 12 contact devices.

YIG magnetometer (P. Nikitin)

P.I. Nikitin[1], P.M.Vetoshko[2] and M.V. Valeiko[1]
[1]General Physics Institute, Academy of Science of Russia
38 Vavilov St., Moscow, 119991, Russia
E-mail: nikitin@kapella.gpi.ru
[2]Institute of Radioengineering and Electronics, Academy of Science of Russia,
11, Mokhovaya St., Moscow, 103907, Russia

Among factors limiting sensitivity of magnetometers those related to the thermodynamic nonequilibrium state in the remagnetisation cycle of the sensing element are very significant. Formation of nonsaturated regions of the sensitive element, domains, domain walls, inhomogeneity at dislocations, etc. can be mentioned foremost. Transition processes during establishing of the equilibrium can also produce irregularities. All the mentioned factors cause the sensitivity decrease and the noise of 1/f - type typical for flux-gate magnetic field sensors. Besides, in strongly nonequilibrium systems an adequate evaluation of the sensitivity threshold of a sensor on the basis of the material parameters is rather problematic.

Many of these problems can be avoided by utilising of rotation of the magnetisation in saturated single domain magnetic films [1-4]. When the total magnetic flux through the film is constant, and the film is in the quasi-equilibrium state, the fluctuation-dissipation theorem [5] and known thermodynamic relations can be adequately used to describe thermal fluctuations and to evaluate the minimal noise level of the magnetometer [4]. Utilisation of saturated monodomain films of substituted YIG for magnetometry wase described in [1] as an alternative to sensing elements with the domain wall motion involved, which usually leads to the Barkhausen jumps (amplitude effect) and the domain walls speed limitation (frequency effect).

In this paper the use of epitaxial yttrium iron garnet (YIG) films in transducers excited by a magnetic field rotating in the film plane is considered. The circular excitation of the film allows one to keep it in the saturated monodomain state and exclude the Barkhausen noise. Using of the ferrodielectric material enables one to avoid eddy-current losses, which limit the excitation frequency and, thus, the magnetometer sensitivity and are also an additional source of noise.

The in-plane and vertical components of the magnetic susceptibility of a YIG single crystal film are analysed. Conditions of simultaneous measuring of three orthogonal magnetic field components by the YIG single crystal film have been established.

A new theoretical approach has been introduced to estimate magnetic noises in a system of coils and a magnetic material, which is in the monodomain state provided by uniform magnetisation rotation. The minimal detectable levels of magnetic field due to noise of the magnetic material and coils are analysed and compared with the experimentally measured values. The prospective way is described to design the magnetometer with noise of several $fT/Hz^{-1/2}$ at room temperature.

To check the developed approach a 3-D magnetometer has been designed. A YIG film was placed inside three plane coils with orthogonal orientation. The coils were pumped with ac current of 30 kHz frequency. The current amplitudes in x- and y-coils were equal and a relative phase shift of 90° was used to produce a uniformly rotating magnetic field H of constant magnitude in the plane of the sample. The impedance values of each coil were measured by a Wheastone half-bridge scheme using a self-made multi-channel vector digital voltmeter. The intrinsic noise for the film evaluated by measurements of magnetic susceptibility was found to be independent on the rotational magnetic field after complete saturation at $H > 10$ Oe. It is to be noted that this value is 5 times as much as the saturation fields revealed by hysteresis loop measurements for the same film. The magnetometer calibration was carried out in a three-layered magnetically screened chamber with extinction ratio of 60 dB by a test uniform magnetic field. The noise level in measurements of each magnetic field component was close to the value published in [4] and was about (0.2 - 1) $pT/Hz^{1/2}$ at frequencies above 0.1 Hz. The value agreed with the

theoretically evaluated for the used core and system of coils. The absence of the 1/f-flicker noise in the band above 0.1 Hz is a substantial improvement in comparison with the best commercially available flux-gate magnetometers. The absence of the flicker noise proves the complete saturation of the magnetic materials at the rotating saturation field of 10 Oe. The flicker noise arose at rotating saturation fields below 10 Oe.

The developed approach of noise analysis shows very promising ways for further improvement of the detection limit, namely, by increasing of operating frequency, Q-factor of coils, filling factor of the coils or magnetic material volume while keeping the film in the monodomain state, by minimising the value of saturation field and "dead" volume of the coil system, etc. The possibility to reach the detection level of cooled SQUIDs looks very feasible with such sensors at room temperature.

REFERENCES

[1] P.M. Vetoshko, V.B. Volkovoy, V.N. Zalogin, A.Yu. Toporov, J. Appl. Phys., 70, p.6298-6300, 1991.

[2] A.Ya. Perlov, A.I. Voronko, P.M. Vetoshko, V.B. Volkovoy, Proceedings of 38th Annual Conference on Magnetism and Magnetic Materials, Minneapolis, Minnesota, Nov. 15-18, paper BR-06, p.128, 1993.

[3] M.V. Valeiko, P.M. Vetoshko, A.Ya. Perlov, A.Yu. Toporov, Solid State Physics, 36, p. 3067-3070, 1994.

[4] M.V. Valeiko, P.M. Vetoshko, P.I. Nikitin, Proceedings of 3rd EMSA Conference, p. 141-142, July 19-21, 2000, Dresden.

[5] L.D.Landau and E.M.Lifshitz, Theoretical Physics, v. 5, Statistical Physics, Moscow, Nauka, 1964.

SQUID "Superconductive Quantum Interference Devices", Physics and Applications (M. Schilling)

Meinhard Schilling
Institut für Elektrische Messtechnik und Grundlagen der Elektrotechnik, TU Braunschweig, Hans-Sommer-Str. 66, D- 38106 Braunschweig, Germany

A superconductive quantum interference device (SQUID) consists of a superconducting ring, which is interrupted by one or more Josephson junctions. Its physical description is based on the Josephson effects, the quantization of magnetic flux in a superconducting loop and the Meissner-Ochsenfeld effect. The SQUID is a sensor for the magnetic flux threading its ring. The voltage response of a SQUID is periodic with the magnetic flux quantum. It measures relative changes of the magnetic flux compared to its flux state during cooling through the superconducting transition temperature. Based on these principles but with different geometry various kinds of SQUIDs have been developed.
Since mixing of external high frequency radiation with the internally generated Josephson currents of high frequency is to be avoided, the SQUID has to be electrically shielded against external electromagnetic radiation.
Very important for practical SQUID design are some guidelines for calculating the involved inductances to combine the SQUID with flux collecting superconducting loops to increase its sensitivity to external magnetic fields. Thus, a superconducting magnetometer consists of a SQUID which is coupled to flux-collecting structures.
The SQUID properties in homogeneous static and time varying magnetic fields are discussed. The electronic parameters sensitivity dU/dB together with dynamic range, noise properties and linearity are of special importance. In its thin film realization the SQUID is a quite ideal vector sensor, which measures only the projection of the ambient magnetic field on the surface normal of the chip.
From the materials point of view the cuprate high-temperature superconductors (HTS) behave differently from the metallic superconductors with respect to their superconducting and magnetic properties as extreme type-II-superconductors. Further consequences of the d-wave superconducting order parameter in the HTS-materials are shortly addressed.

CRYOGENIC OPERATION

Typical conditions in cryogenic systems impose constraints on the operation of the SQUIDs with regard to their thermal, magnetic and vibrational properties. The thermal stability during measurement operation is important, since by a thermal drift excess low frequency noise is generated. The operation of the SQUIDs in a liquefied gas at its boiling temperature guarantees constant temperature if the gas pressure above the liquid-gas surface stays constant. This advantage over other magnetic sensors is given up, if a closed cycle refrigerator is employed as is often required in industrial environment. Despite the problems with cooling small hand-held cryogenic systems for low-noise operation of SQUIDs have already been demonstrated.
Due to the higher operation temperature of 77 K of HTS-SQUIDs the thermal energy in the sensors is higher than in 4.2K-operated niobium SQUIDs and thermal activated phase slippage is important for correct description of current transport at the elevated temperature. The consequences of this on the layout and design of HTS-SQUIDs are discussed.
Since the HTS-materials react rather sensitive on any contact to water a long term stable encapsulation is required to avoid deterioration due to chemical aging, when the sensor warms up and water can condense on its surface.

MAGNETIC ENVIRONMENT

In real world applications the superconducting magnetometer system has to be operated in inhomogeneous magnetic fields of different frequencies. In many applications small magnetic signals have to be resolved on the background of a large static magnetic field i.e. the earth magnetic field. Then all mechanical vibrations of the SQUID are converted to large magnetic disturbances.
For the operation of SQUIDs in high background magnetic field the properties of the superconducting vortex lattice and its behavior in the presence of large shielding currents are equally important. Of special relevance here is the amount of trapped flux in the thin films during the cooling of the device to its working temperature. To minimize this trapped flux, different concepts for the design of SQUIDs have been investigated, which are compared with respect to their ability to suppress the excess noise for operation in large static and dynamic magnetic background fields.
Even in single channel systems often multiple SQUIDs are required, since under most environmental magnetic conditions more then one sensor is necessary to determine magnetic gradients of first and second order. Based on electronic or hardware gradiometry sophisticated noise cancellation schemes have been developed. These allow to distinguish the signal from a large background noise, even if the disturbances are many orders of magnitude stronger.
A special lecture of this fall scholl provides more details of this topic.

APPLICATIONS

Where a magnetic field resolution below 1 pT for a bandwidth of at least 1 kHz is required, due to their very low intrinsic noise, SQUIDs - especially at low frequency - find a market niche as magnetic field sensors and the additional expense for the cooling is acceptable.
Also, for magnetic microscopy SQUIDs show superior performance to other sensors, when moderate spatial resolution with high magnetic sensitivity is required. In a special contribution of this fall school the advantages of SQUID microscopes will be discussed.
Other applications make use of the extremely large dynamic range of SQUID sensors, which can exceed 140 dB. This can be very important if small signal have to be measured in the presence of a large magnetic background field, as in nondestructive evaluation, as discussed in special lectures during this fall school.
Another field of applications is open for the measurement of high frequency magnetic fields. Due to their low inductances SQUIDs are very fast magnetic sensors operating as magnetic field sensors up to frequencies of several Megahertz. This makes them interesting devices for very low noise high-frequency amplifiers. An application here is low field nuclear resonance imaging, which is introduced separately during this fall school.
If many SQUIDs are used in parallel in multisensor systems their mutual interaction with respect to temperature and magnetic fields becomes important. The use of many SQUIDs makes the contemporal mapping of the magnetic field distribution on a sample possible. This is used in large systems for biomagnetic mapping of the activity of the human heart and brain.
These applications are addressed in detail in separate contributions during this fall school.

Giant Magneto-Impedance in Structured Materials for Miniature Magnetic Sensors (L. Panina)

L.V. Panina
Department of Communication and Electrical Engineering, University of Plymouth
Drake Circus, PL4 8 AA, Plymouth, UK

Recent discovery of the magneto-impedance (MI) effect has opened new horizons in the development of micro magnetic sensor technology. MI involves a very large and sensitive change (up to 100%/Oe) in the complex impedance of certain soft magnetic materials. However, with decreasing the sensor element size, the maintenance of such high sensitivity becomes a major concern. Special thin-film structures are employed to improve MI performance in miniature elements. The present lecture concerns the principal advantages of MI in magnetic/metallic multilayered materials. The physical concepts, theoretical analysis based on field-dependent surface impedance matrix and experimental results are discussed. This includes multi-fold enhancement of the MI ratio and a considerable extension of the operational frequency range. Along with this, special types of magnetic anisotropy can be induced in layered systems to realise antisymmetrical and asymmetrical MI. The symmetry property is of a particular interest for magnetic sensor applications. A number of sensor designs are considered.
The lecture is organised as follows

1. It starts with a brief introduction into MI effect introducing the concept of the surface impedance tensor in relation to the voltage response.
2. The next stage is to consider the analysis of MI in multilayers to demonstrate the principle advantages of this geometry. Special attention is given to the role of magnetic anisotropy
3. Then, the experimental methods of measurement of the impedance tensor and principal experimental results are discussed. The use of various alloys is considered.
4. Further, I focus on asymmetry/antisymmetry in MI behaviour, which is very important for linear sensing
5. Finally, a number of MI sensor designs are considered. Special attention is given to implementation of the off-diagonal impedance to realise linear sensing.

Thin Film Magnetoresistive sensors (S. Tumanski)

S. Tumanski, Warsaw University of Technology

PART I: ANISOTROPIC AND GIANT MAGNETORESISTANCE IN THIN FILMS STRUCTURES

a. Essential information about magnetoresistive effects.

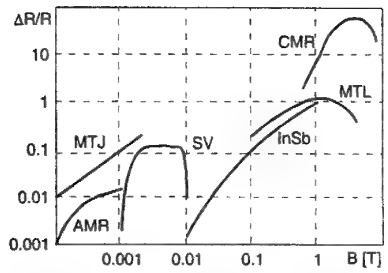

Fig.1. The magnetoresistive effects: AMR – anisotropic magnetoresistance, MTJ – magnetic tunnel junction, SV – spin-valve sensors, InSb – semiconductor magnetoresistors, MTL – multiplayer GMR sensors, CMR – colossal magnetoresistance

b. Anisotropic magnetoresistance – theory and model of the sensor. The structure of the film and stabilization of the magnetoresistive effect. Biasing techniques of thin film – hard magnetic layer, soft adjacent layer, antiferromagnetic layer, dual element sensors. AC biasing techniques. Barber-pole sensors.

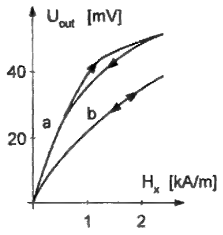

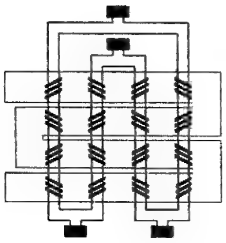

Fig.2. Barber-pole sensor

c. Giant magnetoresistane – an historical review and the main terms. The theory and model of the sensor. Spin valve sensors with asymmetric layer. Spin valve sensors with exchange-based layer. Magnetic tunnel junction sensors. Current perpendicular to plane thin film structures. Colossal magnetoresistance.

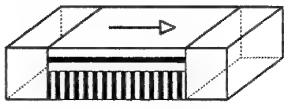

Fig.3. Spin-valve sensor

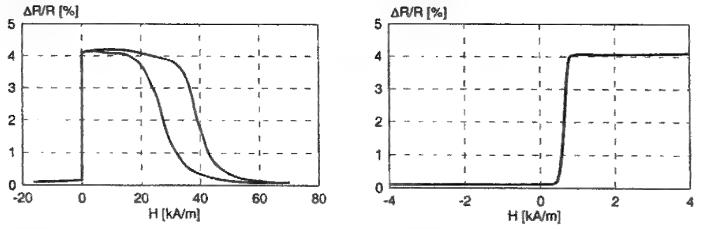

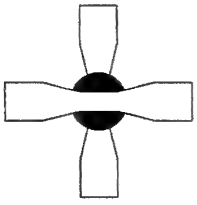

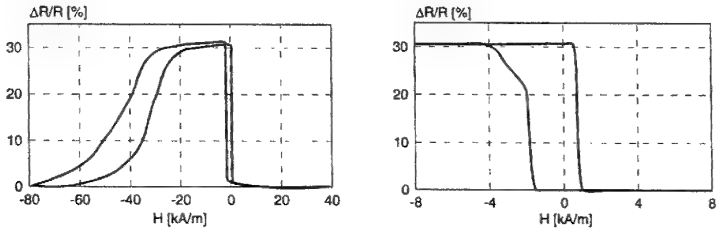

Fig.4. Magnetic tunnel junction sensor

PART II: MR SENSORS – PERFORMANCES AND APPLICATIONS

a. The construction of magnetoresistive sensors.

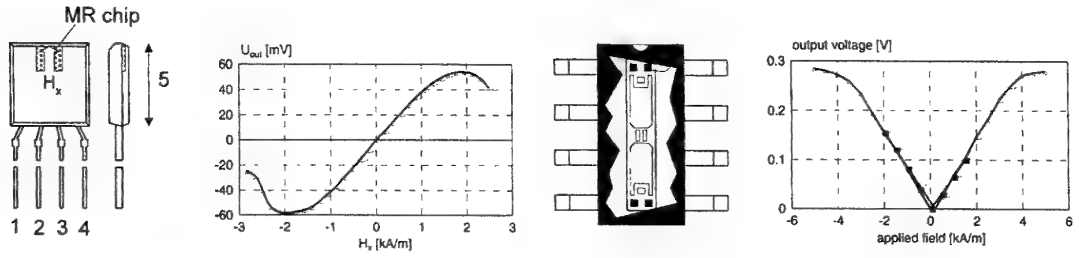

Fig.1. The construction and transfer characteristic of AMR sensor (Philips) and GMR sensor (Nonvolatile El. Inc.)

b. The performances of MR sensors: sensitivity, noise, range, frequency bandwidth, temperature errors, accuracy.

c. The main applications of MR sensors: magnetometers and compasses, electrical transducers: current sensors, electrical power sensors, galvanic isolation devices. Magnetic random access memory (MRAM). Magnetoresitive reading heads. Transducers of mechanical values. Sensors for non-destructive testing of materials.

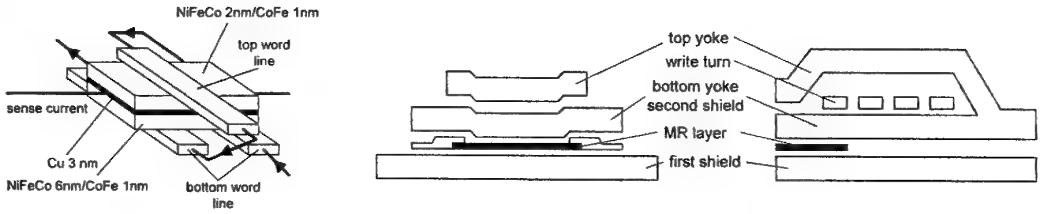

Fig.2. Magnetic random memory element and shielded magnetoresistve reading head

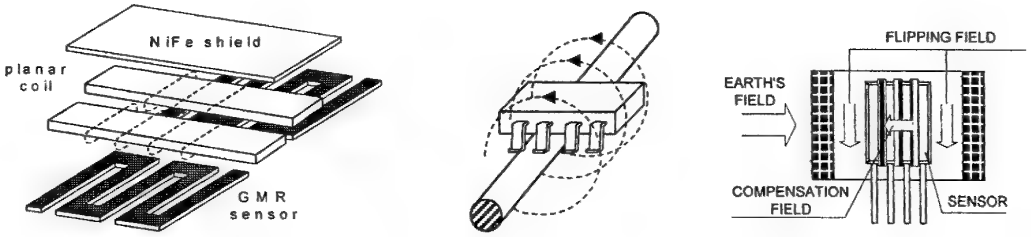

Fig.3. Galvanic isolation device, current sensor, magnetic field sensor

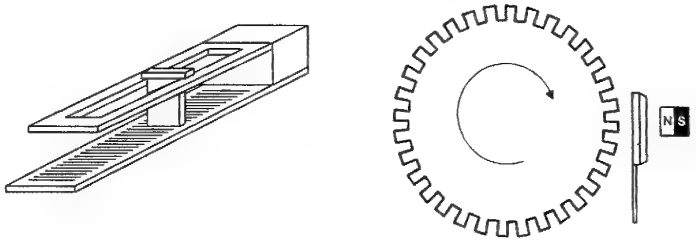

Fig.4. Linear position sensor and sensor of rotational speed

Magneto-optical magnetometry (S. Flament)

S. Flament
GREYC-ISMRA, CNRS – UMR 6072
6, Boulevard du Maréchal Juin 14050 CAEN cedex FRANCE

Magneto-Optical (MO) effects are widely used in the fields of recording and optical telecommunications. In magnetically ordered materials, these MO effects arise from different absorption coefficient and different total contributions to electronic transitions for left and right circularly polarized waves. They lead to the rotation of the plane of polarization of polarized light either crossing a magneto optic material (Faraday effect) or being reflected at its surface (Kerr effect). The measure of this rotation enables an optical non perturbative measurement of flux density.
By the use of magneto-optical indicator showing large faraday effect, very attractive applications are developing like the measure of ac and dc current in high electric field environment or like the imaging of out of plane flux density. This latter application enables detection of buried defects or observation of flux penetration in superconducting samples without scanning.

Magneto-optical indicators are of different shape (bulk crystal or epitaxial thin film) or composition depending on the flux density to measure. Optical and magneto-optical properties of these materials are wavelength and magnetic dependent. How these properties may affect the sensitivity and the dynamical range of the magnetic measurement is explained.

The use of magneto-optical single crystal as current sensors in place of traditional current transformers is shortly presented [1]. The presentation then focused on the description of a typical flux density imaging setup. Namely, parameters fixing both magnetic and spatial resolutions are given. As an example, using YIG ferrimagnetic garnets with in plane anisotropy, a signal to noise ratio of 1 per gauss and per acquisition can be achieved [2].

NDE applications [3] are presented as well as pictures of superconducting single vortices [4] as an illustration of the performance of magneto-optical magnetometry.

REFERENCES

[1] : Magneto-optical properties and sensing performance of garmet YbBi : YIG, W. Zhao, sensors and actuators A89 (2001), pp 250-254

[2] : High resolution magneto – optical imaging of superconducting thin films, S. Flament, Warsito, C.Cordier, L.Méchin and D.Bloyet, IEEE Trans. Appl. Supercond. Vol II,N° 1 , pp 3174-3177 (2001).

[3] : Magneto – optical vizualization of metal loss defects in a ferromagnetic plate : experimental verification of theoretical modeling, M. Shamonin, M. Klank, O.Hagedorn, H. Dötsch, Applied optics Vol 40, N° 19, pp 3182-3189

[4] : Real - time Magneto-optical imaging of vortices in superconducting $NbSe_2$, P.E. Goa, H .Hauglin, M. Baziljevich, E. Il'Yashenko, P.L. Gammel, T.H. Johansen, Supercond. Sci. Technol. 14 (2001), pp 729-731

Fundamentals and Applications of μ Magnetometers (F. Baudenbacher)

Franz Baudenbacher

There have been a number of techniques developed to image magnetic fields at the microscopic level. The techniques include: decoration techniques, magnetoresistive or Hall probe sensors, magneto-optic thin films, Lorentz microscopy, magnetic force microscopy (MFM), scanning electron microscopy with polarization analysis (SEMPA), electron holography (EH) and Superconducting Quantum Interference Device microscopy. The lecture will focus on the fundamentals of each of the techniques, particular how technolgies scale if the sensing volume is reduced in order to increase the spatial resolution and show some of the key experiments which highlight the strength of a particular approach. Furthermore, we will discuss the trade off between spatial resolution and magnetic field sensitivity in the context of possible sample to sensor spacings and charaterisitc scalling propoerties of the magnetic field to be investigated. In addition we describe the experimental approach, the limitations of different techniques and describe which imaging techniques are ideally suited for being used by non specialists.

Noise reduction technic (M. Lam Chok Sing)

Marc Lam Chok Sing
Groupe de recherche en Informatique, Image et Instrumentation de CAEN
6, Bd du maréchal Juin, F-14050 CAEN Cedex

In this talk, I will try to review the different methods commonly used to lower the noise levels of sensors or to improve their signal to noise ratio. Noise adaptation of the sensor to the preamplifier is one of the first operations we usually do to ensure easier signal detection or measurement and this can be obtained through the use of transformers or resonant circuits. The sensor sensitivity can be increased through careful designs, namely the use flux concentrators in SQUID and in magnetoresistive (MR) devices.

Most of the sensors involved in magnetic field measurement suffer from high levels of low-frequency (or 1/f) noise. The origins of such noise for some cases are well established : for example, low-frequency noise in superconducting devices (namely SQUIDs) result from fluctuations of trapped magnetic flux in the film and from fluctuations in the critical current and resistance of the junctions, whereas the noise in MR devices is associated to domain wall fluctuations. Several methods involving the modulation of one (or more) of the device parameters have been proposed and these can lead to a dramatic reduction of the low frequency noise levels. The principle of such modulation and demodulation schemes is readily explained in the frequency domain and can be summarized as follows : the modulation process operates a shift of the sensor response to a higher frequency f_m which is generally chosen in the white noise region, well above the corner frequency ; after some amplification, the demodulation process shifts back the sensor response to its original frequency and the latter is thus recovered. Such modulation schemes result in lower noise levels since the apparent low-frequency noise level correspond to that present around the chosen modulation frequency f_m. Illustrations of these modulation schemes such as the ac current bias and flux modulation commonly used for SQUID magnetometers as well as some other methods for magnetoresistive or Hall effect devices will be given.

Finally, the ultimate way to reduce the noise level is to track it down to its source in order to limit or prevent noise formation. Of course, the quality of the films in which the devices is made is primary factor. Noise in AMR can be lowered by applying stabilizing longitudinal fields. Further reduction in noise have been achieved in SQUID magnetometers by providing the flux concentrators with holes or strip lines of a given maximum width instead of filled structures or by the introduction of flux-dams. Such designs prevent the entrance of vortices into the superconducting films during cooling or when the devices are moved in the earth magnetic field.

APPLICATIONS

Magnetic anomaly detection –Military Applications (Y. Bourez)

Yann BOUREZ
Groupe d'Etudes Sous-Marines de l'Atlantique (GESMA) Brest

GESMA (Groupe d'Etudes Sous-Marines de l'Atlantique) is based in BREST (France). A part of its activities is to study and to control ship magnetic signatures in order to assure, on one hand, the magnetic discretion of French navy ships, and to develop, on the other hand, magnetic detection systems.

Concerning the magnetic discretion of French navy ships, several research ways exist. The first one is to define and to control all ship sources of indiscretion. Indiscretions can be classified in two categories: static indiscretions and alternative indiscretions (0 - 200 Hz approximately). If the first ones are relatively well known, the second ones have just been studied for last years. Actually, a specific interest in "large" bandwidth magnetometers has risen.

The second one is to predict the magnetic signature of a ship everywhere in space from a set of measurements realised on magnetic range. In order to validate the extrapolated signatures, specific magnetic sensors are needed to measure the ship signature from a distance superior to 200 meters in different environmental conditions. These sensors need to be transportable and isotropic. They must be equipped with an integrated security system for data registration or transmission

The third one is to equip ship with onboard systems which are designed to reduce, in real time, the magnetic signature of vessels. They consist of a set of sensors placed near the sources of magnetic anomalies. They control the intensities of a set of degaussing loops regularly placed along the ship. The main point of such sensors is to be precisely time stable.

As it was said before, GESMA is engaged in the development of several magnetic detection systems too. The first system is an airborne detection concept based on an optically pumped 4-helium magnetometer. The sensor, developed by CEA/LETI (Laboratoire d'Electronique et de Technologie de l'Information), is scalar, isotropic and shows a large bandwidth. The prototype will be tested during next year and will be compared with present MAD system based on NMR (Nuclear Magnetic Resonance) sensor.

The second system is a disposable magnetometer buoy. The final purpose is to obtain a kind of deployable net of buoys in order to detect and track underwater target or to check the safety of local areas. Buoys could be deployed by plane or by ship and should be able to transmit their data to a treatment centre. This project has just reached its conceptual step. At this time, an experimental prototype has been developed by ISMRA (Institut des Sciences de la Matière et du Rayonnement). The probe is composed of a 3-helium cell. The concept of the disposable magnetometer buoy is to dissociate the optical pumping (the expensive part of the device) and the measurement probe (the disposable part). The buoy is in fact a two-steps system : firstly, the buoy is optically pumped on board of the deployment platform and secondly, buoy is placed in sea, without pumping device, to measure the ambient magnetic field. The main qualities of such a sensor should clearly be its autonomy and its isotropy.

Finally, it should be said that GESMA possesses several ranges facilities composed of ranges of tri-axis flux gate magnetometers. The first ones are placed in the bay of BREST and are used to measure ship underwater signatures. The second ones are used on earth in order to measure individual signatures of specific ship pieces or different kinds of AUV.

Use of "HiSen" Magnetometers in Geomagnetism (J. Rasson)

Jean L Rasson
Centre de Physique du Globe, Institut Royal Météorologique de Belgique, B-5670 Dourbes, Belgique
jr@oma.be

MAGNETIC OBSERVATORY APPLICATIONS

Principle of Geomagnetic field measurement in Observatory: Components measurements, precautions for HiSen performance. Assessment of accuracies by absolute measurements.
Application of fluxgate magnetometers as variometers, in Difluxes; Vector angles measurements
Particular Problem of automatisation of Observatory measurements
Use of Torsion magnetometers in Observatory practice. Use of Rotating Coil magnetometer
Modulus of field measurement:

Proton Magnetometer, Overhauser, Proton Vector (DIDD)
Optically Pumped Magnetometers (Rb Cs K He), Mz configuration, 4-photon, Self Oscillating Potassium. Assessment of accuracies – constants in Breit-Rabi formula.
OPM Vector (Cs K He)

GEOPHYSICAL PROSPECTION

Magnetometers especially usefull for Hi Res prospection: Proton Magnetometer, Optically Pumped Magnetometers (HFS, Mx, SuperGrad). Desirable features for magnetic prospection.

SEISMOMAGNETICS

The emerging technique of seismo magnetics has used especial magnetometers designed around proton magnetometers, OPM (SuperGrad), torsion magnetometers, fluxgate magnetometers.

MAGNETOTELLURICS

This discipline uses component magnetometers design based on fluxgate magnetometers and search coils. Flux feedback has greatly extended the passband of search coils..

RAPID VARIATIONS

Applications: K-Index, Schumann resonance. Measurement set-ups

OTHER APPLICATIONS OF HiRes MAGNETOMETERS IN GEOPHYSICS

Gravimeters, Rotation detectors

Space Magnetometry (F. Primdahl)

Fritz Primdahl Danish Space Research Institute and Measurement & Instrumentation, Oersted·DTU, Technical University of Denmark, Building 327, Elektrovej, DK-2800 Kgs. Lyngby, Denmark. fpr@oersted.dtu.dk 10/10 2002FP

INTRODUCTION

General requirements for high-performance space instrumentation concern robustness against the launch shocks and vibrations, the rapid pressure drop from 1atm to near-perfect vacuum and vacuum-thermal balance design in the absence of heat transport by air convection. Reliability is a particular issue, because of the cost per kg of putting instrumentation in Earth orbit or into deep space and because of the post-launch inaccessibility. Longevity may be assessed by accelerated lifetime tests at substantially elevated temperatures, thermal stress durability is tested by temperature cycling the equipment repetitively through the full temperature ranges. Radiation resistance must be tested statistically by batch circuit samples destruction, often in-house, because manufacturer-specified rad-hardness and space-qualified components are extremely high-priced and the available circuits often outdated. For new developments modern circuits as a rule do not exist in space-qualified versions and so you have to do your own space qualification. Instrument autonomy and redundancy become critical performance parameters, and in-operation monitoring of circuit test points via housekeeping telemetry becomes indispensable as a diagnostics and remote servicing tool. These general considerations for space instrumentation are thoroughly treated in a number of tutorial texts [see e.g. Fortescue and Stark, 1997] and will not be repeated here. The following, therefore, deals with the particular demands posed by magnetic measurements onboard satellites, and the efforts needed to solve the measurement tasks, be it for attitude purposes or for high-precision mapping of planetary or deep space magnetic fields.

INSTRUMENTATION

The most common request is for continuous monitoring in a low Earth orbit of the vector magnetic field components relative to the spacecraft coordinate frame for S/C **attitude determination**. This requires a tri-axial magnetometer, and depending on the applications the accuracy may be from 0.1°-1° corresponding to an accuracy of 87nT to 870nT in an environmental magnetic field of 50 000nT. Magneto resistors, Hall probes or Fluxgate transducers [Ripka, 2000] may have the calibration and zero-level stability to provide such attitude accuracies, and the main concern then becomes the local static and dynamic magnetic perturbations from the host spacecraft. For **planetary magnetic field mapping** the requirement is typically <1nT accuracy per component and a determination of the absolute orientation of the magnetometer sensor to comparable accuracy, i.e. 1nT relative to 50 000nT or better than 4 acrseconds. This requires a fluxgate magnetometer of extreme linearity and extended dynamic range [Nielsen *et al.*, 1995] in combination with a star camera system [Jørgensen, 2000]. Full control of the zero level stability and the scale values of a field mapping magnetometer often requires in-flight calibration by comparison to an onboard absolute scalar magnetometer [Primdahl, 2000], which may be a nuclear resonance magnetometer or an electron spin resonance instrument using optical pumping. As is the case for the attitude magnetometers, the local magnetic perturbations from the host spacecraft become a serious contribution to the measurement errors. These are reduced to a tolerable level by the combination of implementing a magnetic cleanliness program for the host satellite and placing the magnetometer sensor at the tip of a boom, as far away from the perturbations as possible. On **deep-space missions** the magnetic fields encountered are about 50nT or lower, and so the demands for stability of the scale values and the absolute orientation knowledge are correspondingly relaxed. However, extreme zero level stability and

very low sensor noise become the driving parameters, also because the addition of an auxiliary absolute calibration instrument for several reasons becomes impossible. The control of the host spacecraft magnetic perturbations will be even more important than for planetary mapping missions, because the natural deep-space fields and field fluctuations are considerably lower.

THE S/C MAGNETIC CLEANLINESS ISSUE

Reducing the magnetic field from a satellite is, in essence, no different from reducing the weight or power. Early in the design phase the issue has to be considered, and the magnetic field sources (static and dynamic) have to be identified, measured and, if possible, reduced. Two types of magnetic field sources dominate: magnetic materials in components and structural parts, and electric currents flowing in e.g. power supply wires and the structure. The first can be measured in terms of their magnetic moment (in $A \cdot m^2$) by a magnetometer and reduced by selecting non-magnetic alternatives where possible, and the latter is controlled by twisting the wires in parallel with using clever grounding schemes to avoid uncontrolled structural return currents [Primdahl, 1990]. Other advanced methods are used in the situations where these simple first approaches do not lead to sufficiently low perturbations.

BOOM DEPLOYMENT OF THE SENSORS

Generally, the perturbation fields from magnetic materials and components dominate over the fields from unbalanced electric currents, and one or two diameters away from the satellite the perturbation field drops off as the third power of the increasing distance like a dipole field. This means that the perturbation field drops a factor of 8 for every doubling of the distance from the spacecraft center of gravity. Deploying the magnetic sensor on a boom is therefore a most cost effective way to reduce the magnetic perturbation field at the sensor. Combining a reduced magnetic cleanliness program for the satellite with a moderate length boom often leads to a technically acceptable solution meeting the measurement accuracy requirements. Reduction of the spacecraft dc and ac perturbation fields in the data is often possible by placing a second magnetometer sensor about half way in on the boom, because the two magnetometers see the same external field, but the inboard magnetometer sees about 8 times larger spacecraft field than does the outboard sensor.

END-TO-END SYSTEMS CALIBRATIONS

Some level of calibration of the magnetometer is important for all types of magnetometers. The required measurement accuracy determines the efforts put into the calibration. Particularly important is the end-to-end calibration of the magnetometer integrated in the spacecraft and with the data taken through the satellite telemetry and under timing control of the onboard system.

UNIT LEVEL MAGNETIC CALIBRATION

Calibration at flight instrument stand-alone level is performed as part of the instrument tests. It consists in determining the parameters of a mathematical model chosen to describe the sensor and electronics performance. It may be a simple linear model with 3 offsets, 3 deviation angles from orthogonality and 3 scale values, it may include the temperature coefficients of these parameters, or it may be a full spherical harmonics modeling of the single axes' non-linearities and off-axis deviations [Risbo *et al.*, 2002]. The calibration can be performed in a tri-axial test coil system, where the Earth's field is compensated for and the test fields are generated under computer control. It may also be performed in the unperturbed Earth's field by recording the sensor outputs for a suitable number of fixed orientations [Merayo *et al.*, 2000], the number depending on the complexity of the sensor response model.

ATTITUDE SYSTEM - MAGNETIC SENSOR INTERCALIBRATION

The parameters of the chosen model determine the intrinsic magnetic axes of the sensor. Special actions have to be taken to make these axes externally accessible. For attitude magnetometers the machining and production accuracy is often sufficient to ensure that the magnetic axes are within 0.1° - 0.5° of the direction of the edges of the sensor housing. For stable high-precision axes determination optical quality mirrors are clued to the sensor structure, at least two externally accessible mirrors having about 60° - 120° between their normals are needed. Repeated rotations of the sensor about the mirror normals in the Earth's field or in suitable coil system fields are used to determine the optical mirror normals' directions in the intrinsic magnetic coordinate system of the sensor. For the high-precision star camera magnetometer sensor system mounted on a stable optical bench, the relation between the camera bore-sight and CCD chip axes and the sensor magnetic axes is determined in the unperturbed Earth's field at an Astronomical Observatory by letting the camera view the clear night star sky, while the magnetometer at the same time measures the known Earth's field [Risbo and Olsen, 1996].

S/C LEVEL CALIBRATIONS

Important for attitude magnetometers and more so for the high-precision instruments, are the determination of the spacecraft residual magnetic perturbation on the sensor in the deployed flight configuration, and the influence of the spacecraft on the calibration parameters and the noise level of the instrument. This may be done in a large industrial tri-axial coil facility accommodating the entire satellite or, for μ-satellites, in the unperturbed Earth's field by repeated rotations about the satellite payload frame axes [Primdahl *et al.*, 2002].

IN_FLIGHT CALIBRATIONS

Post-launch and after the instruments commissioning phase, an in-flight test of the pre-flight calibration parameters are performed. For the attitude magnetometer, using the satellite position and an alternative onboard attitude system may do this by comparing the magnetometer output to the IGRF model of the Earth's field. For the high-precision magnetometers this is done by comparison to the onboard absolute scalar magnetometer [Olsen *et al.*, 2002] or by other sophisticated statistical methods.

DATA TIMING ISSUES

Equally important as the selection of a good model describing the sensor and the determination of the correct model calibration parameters is the determination of the exact timing of the individual magnetic vectors measured. This is part of the end-to-end test of the magnetometer onboard the satellite. This may be done by observing a low frequency magnetic field generated by a coil system and comparing the timing of the generator curve with the time tags of the measurements received through the satellite telemetry.

REFERENCES

Fortescue, Peter and John Stark (editors), *in* **Spacecraft Systems Engineering**, John Wiley and Sons, England, 1997.

Jørgensen, John Leif, In Orbit Performance Of A Fully Autonomous Star Tracker, **ESA SP-425**, pp. 103-110, 2000.

Merayo, J.M.G, P. Brauer, F. Primdahl, J.R. Petersen and O.V. Nielsen, Scalar Calibration of Vector Magnetometers, **Meas. Sci. Technol.**, **11**, 120-132, 2000.

Nielsen, O.V., J.R. Petersen, F. Primdahl, P. Brauer, B. Hernando, A. Fernandez, J.M.G. Merayo, and P. Ripka, Development, Construction and Analysis of the "ØRSTED" Fluxgate Magnetometer, **Meas. Sci. Technol.**, **6**, 1099-1115, 1995.

Olsen, N., L. Tøffner-Clausen, T. J. Sabaka, P. Brauer, J.M.G. Merayo, J.L. Jørgensen, J.-M. Léger, O.V. Nielsen, F. Primdahl and T. Risbo, Calibration of the Oersted Magnetometer, **Earth, Planets and Space**, (submitted), 2002.

Primdahl, F., A Pedestrian's Approach to Magnetic Cleanliness, **DRI 2-90**, Danish Space Research Institute, Juliane Maries Vej 30, DK-2100 Copenhagen Oe, Denmark, 1990.

Primdahl, F., Resonance Magnetometers, in: Pavel Ripka, (editor), **Magnetic Sensors And Magnetometers**, **Ch. 7**, ARTEC HOUSE INC., Boston, 2000.

Primdahl, F., P.Brauer, J.M.G. Merayo, J.R. Petersen and T. Risbo, Determining the Direction of a Geometrical/Optical Reference Axis in the Coordinate System of a Tri-Axial Magnetic Sensor, **Meas. Sci. Technol.**, (submitted), 2002.

Ripka, Pavel, (editor), **Magnetic Sensors And Magnetometers**, ARTEC HOUSE INC., Boston, 2000.

Risbo, Torben and Nils Olsen, Attitude Intercalibration of the Star Imager and the Spherical Compact Sensor Magnetometer for the Ørsted Geomagnetic Satellite Mission, **Proceedings of the SPIE – The International Society for Optical Engineering**, **2810**, 230-238, 1996.

Risbo, T., P. Brauer, J.M.G. Merayo, O.V. Nielsen, J.R. Petersen, F. Primdahl and N. Olsen, Ørsted Calibration Mission: The Thin Shell Method and the Spherical Harmonics Analysis, **Meas. Sci. Technol.**, (submitted), 2002.

Non-destructive testing and evaluation of materials using magnetic sensors: Surface and surface near defect detection (A.Yashan)

Andriy Yashan
Fraunhofer Institute for Non-destructive Testing, IZFP,University Building 37, 66123 Saarbruecken, Germany
Email: yashan@izfp.fhg.de

Magnetic sensors can be used for the detection of defects (geometrical discontinuities like cracks or inclusions) in ferromagnetic and / or electrically conductive materials. By using the magnetic flux leakage (MFL) technique for defect detection, a specimen under test is magnetised by the applied static magnetic field of a permanent magnet or an electromagnet system and a magnetic sensor measures the changes of the external magnetic field correlating to the specimen defects. In the eddy current (EC) technique, the time-alternating electromagnetic field is excited in test specimen.

The sensitivity of a non-destructive testing (NDT) technique can be characterised by the smallest detectable defect. The sensitivity of MFL or EC technique depends on the sensitivity of the used magnetic sensor and of the measurement equipment (noise level, dynamic range) but also on the complexity of the testing situation, especially on the presence of disturbing influences which also affect the magnetic measurement (for example, variations of the sensor lift-off during the measurement or inhomogenity of the magnetic or electric properties of the specimen). The choice of the sensor type and the optimal design of the sensor strongly depend on the application. The following paper describes sensor arrangements for selected applications from the experience of the IZFP Saarbuecken.

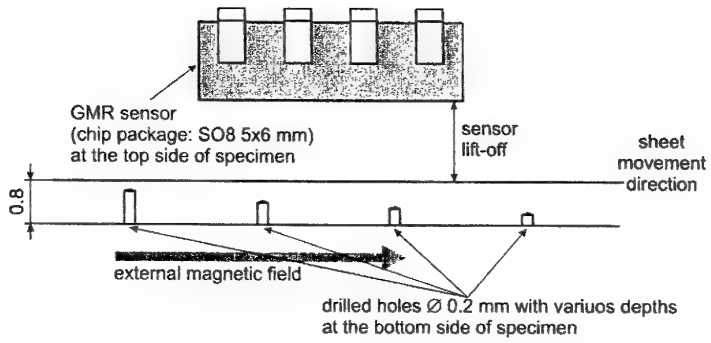

Figure 1

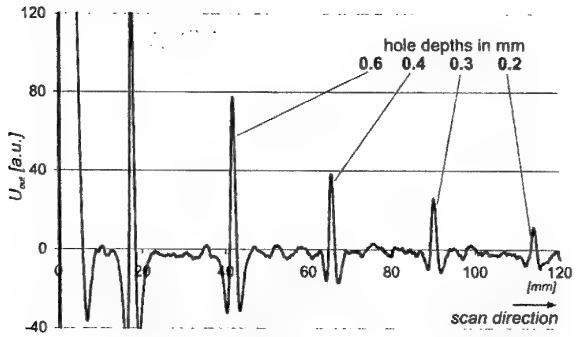

Figure 2

For the on-line high-speed detection of inclusions in cold rolled steel strip (thickness 0.8 mm) the MFL technique using GMR gradiometer [1] has been used (see Figure 1 for the sensor-to-specimen arrangement). The optimisation objective has been to maximize the sensor lift-off. As the results presented in Figure 2 show, the defined artificial smallest detectable defect (drilled hole with a diameter of 0.2 mm and depth 0.2 mm) can be reliably detected with the GMR sensor lift-off of 1.5 mm [2].

The so called multi-frequency EC technique (MFEC technique) is the processing of the EC measurement data - real and imaginary part of the sensor impedance - obtained by inspection applying more than one EC frequency. Disturbing influences like sensor lift-off and tilt or material property discontinuities can be eliminated using MFEC technique with suited calibration, e.g. in order to increase the probability of defect detection or to improve the accuracy of the defect sizing.

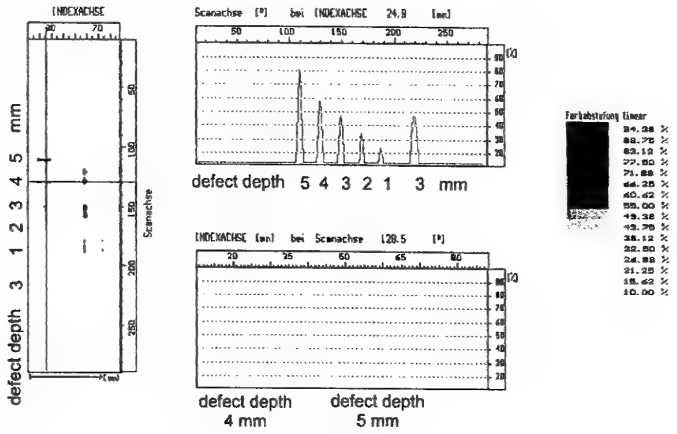

Figure 3

Figure 3 demonstrates the results of the MFEC technique applied for the detection and sizing of the surface-breaking flaws in the stainless steel cladding of a nuclear power plant pressure vessel [3]. An induction sensor has been used. The operating frequencies have been 50 / 280 / 600 kHz. Having a sensor riding at the surface, the grey-scaled C-scan image on the left side of Figure 3 is visualizing the locations and the depths of the notches. The numerical filters here applied suppress interference signals caused by lift-off- and δ-ferrite influences and their local changes. The individual notch depths along the scan paths selected by the cursors are indicated in the amplitude versus scan position representations at the right hand side of Figure 3.

REFERENCES

[1] Product Information Nonvolatile Electronics (NVE) Inc., WWW: http://www.nve.com

[2] A. Yashan, R. Becker, A. Klein, "Detection of small inclusions in thin steel sheets by magnetic flux leakage technique", 8th European Conference Non-Destructive Testing (8th ECNDT), Barcelona, June 2002

[3] R. Becker and M. Kröning, Low Frequency Eddy Current Inspection for Surface and Subsurface Defects of the RPV-Cladding by a New DSP Controlled Eddy Current System, 14th International Conference on NDE in the Nuclear and Pressure Vessels Industries 24-26 September 1996, Stockholm, 335-340 (1997)

NDE: Buried defect detection using sensitive magnetometers (M. Kreutzbruck)

K. Allweins, G. Gierelt, H.-J. Krause and M. v.Kreutzbruck
Institute of Applied Physics, Justus-Liebig-University Giessen, 35392 Giessen, Germany

Over the past few years, sensitive magnetic field sensors have been implemented with remarkable success in eddy current testing (ECT). Conventional techniques using inductive coil systems to measure the magnetic field response have been gradually replaced by alternative sensors, such as flux-gates [1], giant magnetoresistive sensors and in a few applications by SQUIDs [2, 3]. Flux-gates and SQUIDs provide a combination of high field sensitivity at low frequencies and an outstanding high dynamic range. Sensitives fluxgate probes e.g. provides a field sensitivity of a few $pT/\sqrt{Hz}$ at low frequencies and a high dynamic range of more than 140 $dB/\sqrt{Hz}$ which enables one to detect minute or deep lying defects in the structure, component or material being tested [4].
But just because magnetic sensors have a low intrinsic noise level, they do not automatically guarantee reliable crack detection. Because of their high degree of sensitivity, they measure all electro-magnetic interference. In the case of an EC measurement, interference can arise from three sources:

(i) external noise, though this is the least significant factor,
(ii) EC effects created by the sensor head's artificial movement (eg. vibration, tilting and Lift-Off effect),
(iii) EC effects arising from the sample itself.

The latter accounts for the most significant noise factor in the case of complex samples. Due to the skin effect, difficulties arise when testing such samples, which can include edges, holes or a number of various materials close to their surface. The induced EC density is higher at the sample's surface than it is at deeper levels, giving rise to significant distortion currents at the surface near components with differing electrical conductivity. This in turn results in strong variations of the magnetic field distribution above the sample's surface. Thus in many NDE applications the sensors high field sensitivity can only be exploited through the use of additional signal processing, whereby defect-induced field variations are separated from any type of superimposed background signal.

To prevent EC interference caused by the make-up of the sample itself, the detection of deep-lying cracks requires the additional use of sophisticated excitation schemes with adapted coil geometries to decrease the EC density at the sample's surface. This reduces the influence of any bolts or rivets inside the sample and allows for easier defect signal extraction from superimposed background.
Besides an introduction with useful theoretical background of electromagnetic testing the lecture gives an overview of current NDE applications in which sensitive magnetometers and adapted excitation geometries are applied.

REFERENCES

[1]J. Pavo et al., "Eddy Current Testing with Fluxset Probe", Studies in applied Electromagnetics and Mechanics, vol. 12, IOS Press, Amsterdam, S. 215-222, 1997.
[2]J.P. Wikswo Jr., "SQUID magnetometers for biomagnetism and nondestructive testing: Important questions and initial answers", IEEE Trans. Appl. Supercond., 5(2): 74-120 (1995).
[3]R. Hohmann, M. Maus, D. Lombarski, M. Grüneklee, Y. Zhang, H.-J. Krause, H. Bousak and A.I. Braginski, "Aircraft Wheel Testing with Machine-Cooled HTS SQUID Gradiometer System", IEEE Trans. Appl. Supercond. vol. 9, No. 2 (1999), pp. 3801.
[4]M. Mück et al., "Nondestructive Testing of Niobium Sheets for Superconducting Resonators", to be published in IEEE Trans. Appl. Supercond (2002).

MagnetoEncephalography (J. Vrba)

Jiri Vrba
CTF Systems Inc., A subsidiary of VSM MedTech Ltd., Port Coquitlam, B.C., Canada

The magnetoencephalography (MEG) is a discipline concerned with detection and interpretation of magnetic fields produced by human brain. It is a relatively new field, even though the detection of electromagnetic activity of the human brain has a long history. The electroencephalogram (ECG) was first measured in 1929 and its magnetic counterpart, MEG, was first recorded in 1968, using room temperature coils. The further progress in MEG required more sensitive detectors of magnetic fields, which fortunately become available in 1964, shortly after the discovery of the Josephson effect in 1962. These high sensitivity detectors are based on superconducting and quantum phenomena and are called SQUIDs (Superconducting Quantum Interference Devices). The SQUIDs were first used for detection of MEG in 1972. After this pioneering work, the field of MEG developed first by using single channel devices, following by somewhat larger systems with 5 to 7 channels in mid 80s, then systems with 20 to 40 sensor arrays in late 80s and early 90s, and finally the first helmet MEG systems were introduced in 1992. Present day MEG systems have several hundreds channels in a helmet arrangement and operate in either sitting or supine positions.

In addition to MEG, the magnetic signals were also detected from other body organs, e.g. heart, eye, stomach, small intestine, skeletal muscles, peripheral nerves, fetal heart, fetal brain, lungs, etc. However, so far the most important application of the biomagnetism has been to the brain and the MEG started intense technological development in low noise multichannel magnetic detection an lead to the establishment of several commercial suppliers.

The MEG measurements span frequency range from about 10 mHz to 1 kHz (or perhaps as low as 1 mHz for sleep studies) and the field magnitudes from about 10 fT for spinal chord signals to about several pT for the brain rhythms. To appreciate how small the MEG signals are, it should be recalled that the Earth field magnitude is about 50 μT and the urban magnetic noise about 10 nT to 1 μT, or about factor of million to billion larger than the MEG signals. Such large differences between the signal and noise demand noise cancellation with extraordinary accuracy. The noise is usually reduced by a combination of shielding, reference methods (synthetic gradiometers or adaptive), and spatial filtering.

The existing commercial MEG instruments are based on low temperature SQUIDs. Systems based on high temperature superconductors are also being developed, however, mostly for magnetocardiography (MCG) applications. The present high temperature SQUIDs cannot be reliably manufactured in large quantities and are not as sensitive as their low temperature counterparts. However, their performance is steadily improving and they already are suitable for some applications.

The MEG (or EEG) measures magnetic fields (or potentials) on the scalp surface. However, the brain current distribution, which is responsible for the observed fields, is usually more interesting to the user. Unfortunately, the inversion problem (computation of the current distribution from the measured magnetic field) is non-unique and ill-posed and the MEG data must be supplemented by additional information, physiological constraints, or mathematical models and simplifications. Additional information to assist the field inversion can be supplied by other measuring modalities, for example fMRI, MRI, PET, etc. In summary, the MEG (and EEG) provide direct measure of the neuronal activity with excellent temporal resolution, but spatial localization dependent on the non-unique inversion problem. In comparison, the fMRI, PET, and SPECT are limited by the long time constants of the metabolic and hemodynamic processes and by the poorly defined relationship between them and the neuronal processes.

Recently, MEG has also been applied to monitoring brain activity of human fetus and this novel application is called fetal magnetoencephalography (fMEG). Presently, there is no other technique available for assessment of the fetal neurological status. The fMEG has a potential to assist physicians to make informed decisions during high risk pregnancies and diagnostics associated with infection, toxic insult, hypoxia, ischemia, and hemorrhaging.

The fMEG array is shaped to cover the maternal abdomen, roughly from the breast-bone to perineum and it contains 151 sensing channels. Mother sits on and leans against the sensitive end of the dewar. The primary sensors are radial gradiometers with 8 cm baseline and noise is cancelled by 3rd-order synthetic gradiometers.

The measurement of fMEG is a difficult task, because the fetal brain signals are small in comparison with the adult signals, and further, the detection is performed in the presence of strong interference from the maternal and fetal hearts and various abdominal signals (intestinal electrical activity, uterine contractions, etc.). Numerous methods can be used for separation of small fMEG signals from the interference: principal component analysis, independent component analysis, nonlinear dynamics, and signal space projection. Spatial filtering is still problematic as the fetal brain models are not yet well developed. Two extreme fetal brain models can be used: In one extreme, the fetal head is assumed to be completely permeable to electric currents and the fetal brain and the maternal abdomen form an electrically uniform medium. In the opposite extreme, the fetal head is assumed to be electrically impermeable and the brain currents are completely enclosed within it. The truth is probably somewhere in between these two models. In addition to separating the fMEG signals from various artifacts due to the physiological sources discussed above, it is necessary to eliminate artifacts due to fetal and maternal motion. In spite of these difficulties, good quality recordings of fetal brain magnetic activity were obtained. These recordings include auditory and visual evoked fields and spontaneous fetal brain signals.

The use of MEG for detection of brain signals has been successfully demonstrated and MEG is penetrating into clinical application. The MEG has high sensitivity (provided by the SQUID detectors), efficient noise cancellation, and the ability to measure the brain signals on msec scale. Interpretation of MEG data is complicated by the fact that the solution for the three-dimensional current source distribution in the brain from an array of sensors outside the head is non-unique. However, useful source estimates can be obtained after incorporation of additional constraints or assumptions, or alternately, signals from different parts of brain can be isolated by spatial filtering. These features allow MEG to be used for functional neuroimaging of events that are not accessible either to functional MRI or to nuclear imaging methods.

Magnetocardiography (M. Ter Brake)

H.J.M. ter Brake, University of Twente, The Netherlands

Currents flowing within the heart tissue generate magnetic fields that can be detected outside the human body: magnetocardiography (MCG). More traditionally, potential differences on the body surface can be recorded, which is electrocardiography (ECG). MCG-recordings look very similar to ECG-recordings: A normal heart cycle starts with the contraction of the atria (P-wave in the cardiogram), followed by the contraction of the ventricles (QRS-complex in the cardiogram). Relaxation of the ventricles gives the so-called T-wave. Usually, the relaxation of the atria coincides with the contraction of the ventricles and cannot be recognized in the cardiogram as it is obscured by the relatively large QRS-complex. Usually, the largest peak in the heart signal is the QRS-complex that, for adults, is typically about 100 pT in amplitude.

ADULT MAGNETOCARDIOGRAPHY

Research is performed to use adult MCG for distinguishing healthy subjects from patients suffering from various categories of heart diseases (e.g., ischemia). For that purpose, the MCG is recorded at about 30 to 40 positions over the subject's chest. The recorded signals are processed and presented in a variety of plots, e.g. iso-field plots and current-density maps. In a number of studies worldwide, data is gathered to develop criteria for separating healthy and unhealthy subjects. Once a field distribution is obtained, one can try to localize currents within the heart that generate the field (the so-called inverse problem). For some defects, e.g. additional current pathways, this localization may be used to prepare surgery. However, in order to localize a source with acceptable accuracy, a model is required to describe the human body around the heart in terms of a volume conductor. The acceptable system noise in these measurements is 20 $fT/\sqrt{Hz}$ in the measuring band 1–100 Hz. Because of the required resolution, low-T_c SQUIDs are applied with second-order gradiometers.

Apart from any Japanese activity, two companies should be mentioned with regard to adult MCG: Cardiomag Imaging Inc. in the USA (www.cardiomag.com), and SQUID AG in Germany (www.SQUID.de). To the author's opinion, the former is most realistic in estimating the medical relevance of MCG, at present: "CMI, while most encouraged by the data's preliminary indications makes no claims as to the diagnostic value of MCG techniques" (CMI brochure). This diagnostic value still has to be proven.

FETAL MAGNETOCARDIOGRAPHY

Nowadays, fetal surveillance in hospital is based on ultrasonography, including 3D-techniques and echo/Doppler. These ultrasonographic techniques are able to monitor the anatomy and mechanical activity of the fetal heart. The underlying electro-physiological processes in the fetal heart are not recorded. As an alternative, the fetal electrocardiogram can be recorded by means of electrodes attached at the maternal abdomen. The reliability of this straightforward approach, however, is quite poor and furthermore on average the resolution is too low for clinical purposes. This is mainly caused by the fact that, during a relatively long period of the pregnancy, the foetus is more or less electrically insulated from the mother because a fatty layer surrounds the foetus. Fetal magnetocardiography (fetal MCG) might be the solution for this problem.

At the University of Twente, the FHARMON project was started in 1997 (abbreviation for Fetal Heart Monitor). As part of that project, magnetocardiograms are recorded from foetuses with various heart

defects, one of which is the so-called AV-block. A crucial element in the heart cycle is the AV-node that conducts the atrial impulse into the ventricles. Poor conduction through this node generates an AV-block, of which three degrees are distinguished. In the first degree, every pulse is conducted through but with some delay. This results in an increased PR-time interval. In the second degree, not every pulse passes the AV-node. It takes two or more atrial impulses to stimulate the ventricular (QRS) response. In a two to one block, two P-waves show up followed by a single QRS-complex. Finally, in the third degree none of the atrial impulses is conducted through the AV node. As a result, the ventricles or AV node are stimulated by an ectopic pacemaker and the atria and ventricles operate fully asynchronously (complete heart block). Two illustrative case of fetal AV-blocks are given in the figure below.

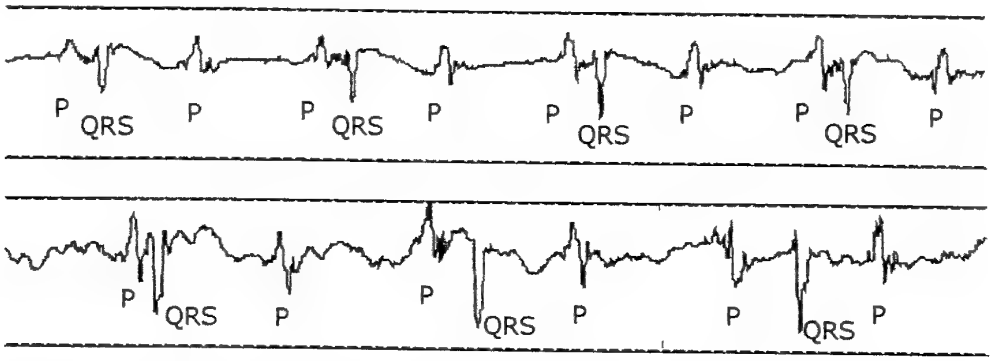

AV-blocks recorded in fetal MCG (36th week of gestation); top: 2nd degree; bottom: 3rd degree.

The main clinical relevance in fetal MCG appears to be in peak durations and intervals. Mapping or volume conductor modeling, therefore, is not of prime interest. In practice, it will be adequate to measure the field simultaneously at a few positions (e.g. 3), but at each position a number of independent field components will need to be recorded. The required resolution is better than 10 fT/√Hz, in the frequency band 1-200 Hz. In unshielded environment, this implies the need of a third-order gradiometer.

CONCLUSION

In conclusion, the advantage of adult MCG over adult ECG still has to be proven. Studies on this topic are in progress. Fetal MCG has clear advantages over alternative techniques as ultrasound and ECG. Here, the challenge is to show the market potential (i.e. to show clinically relevant applications) and to develop a measuring system with adequate resolution for use in unshielded hospital environment.

Others Biomagnetic application:, SQUID System for Biological Immunoassays (K. Enpuku)

K.Enpuku
Department of Electronics, Kyushu University, Fukuoka 812-8581, Japan

Highly sensitive magnetometer system that utilizes superconducting quantum interference device (SQUID) has been developed for the application to biological immunoassays [1]-[5]. In the immunoassays, an antigen, such as pathogenic bacteria, cancer cell or environmental injuries, is detected with its antibody. In order to measure the binding reaction between antigen and its antibody, the antibody is labeled with a magnetic marker made of Fe_2O_3 nanoparticles as shown in Fig. 1(a). A few Fe_2O_3 nanoparticles are embedded in the polymer, and the antibody is attached around the surface of the polymer. In the typical case of commercial maker, the size of polymer is less than 100 nm, and the size of Fe_2O_3 nanoparticles is 10-15 nm in diameter.

The binding reaction can be magnetically detected by measuring the magnetic field from the magnetic marker. In Fig. 1(b), SQUID system is schematically shown. Sample is an assembly of magnetically labeled antibody. The sample size is typically 2 mm in diameter. In order to magnetize the sample, the excitation field B_{ex} is applied in parallel to the SQUID. Then, a signal field is produced from the nanoparticles. The vertical component of the signal field is detected as a signal flux Φ_s.

Since the signal flux Φ_s rapidly decreases with the distance h from the sample, it is necessary to set the SQUID close to the sample. The distance h should be less than a half of the sample size, e.g. h<1 mm. In order to realize the small distance between the SQUID (T=77 K) and the sample (T=300 K), a Dewar similar to the SQUID microscope is used.

Three methods have so far been developed for the detection of the magnetic signal from the marker, i.e., dc susceptibility, relaxation and remanence measurement. We briefly describe these methods.

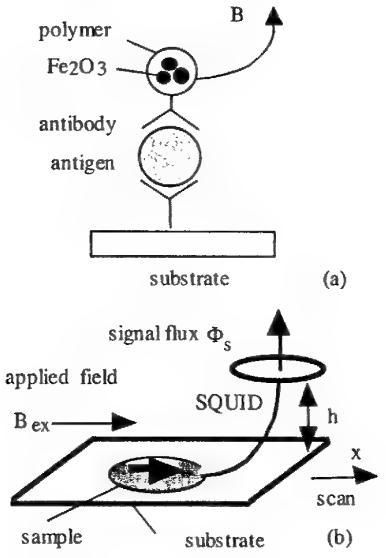

Fig. 1. Principle of SQUID immunoassays. (a) Detection of binding reaction between antigen and its antibody with magnetic marker. (b) Measurement system.

(1) DC susceptibility measurement

The first one is to measure the magnetization of the marker in the presence of dc excitation field [1], [2]. In this case, the dc excitation field B_{ex} is applied in parallel to the SQUID, and the sample is scanned in the x direction with a typical speed of 10 mm/s. In Fig. 2, waveform of the detected signal is shown. The signal flux is detected when the sample passed beneath the SQUID. The peak value of the detected signal gives the signal flux Φ_s.

Since the signal flux Φ_s increases in proportion to B_{ex}, it is preferable to use the large excitation field. However, degradation of the SQUID performance occurs when the field B_{ex} becomes too large. This degradation is caused by the mechanical misalignment between the SQUID and the direction of the field B_{ex}, i.e., vertical component of B_{ex} due to mechanical misalignment degrades the SQUID performance. Therefore, compensation of the vertical component of B_{ex} is important in order to increase the excitation field B_{ex}. At present, the field of B_{ex}=3 mT can be applied without the degradation of the SQUID performance.

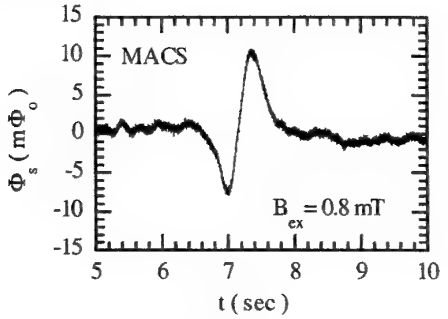

Fig. 2. Waveform of the detected signal when the sample is scanned in the presence of dc excitation field B_{ex}.

The binding reaction between the antigen and its antibody is detected with this method. It is shown that the method can detect the reaction 10 times more sensitively than the conventional optical method [2].

(b) Relaxation measurement

The second method is to measure the relaxation of the magnetization after the excitation field is turned off [3], [4]. Since the size of the Fe_2O_3 particle is typically 10-15 nm in diameter in the case of the commercial marker, thermal noise at T=300 K easily causes the relaxation of the magnetization. In Fig. 3, the experimental result reported in ref. (4) is shown. In the experiment, the excitation field of B_{ex}=0.3 mT is applied for τ_{mag}= 1 s in order to magnetize the sample. After the field is turned off, the magnetic flux of the sample $\Phi(t)$ rapidly decreases with time, whose dependence is given by

$$\Phi(t) = \Phi_s \ln(1 + \tau_{mag}/t) \qquad (1)$$

Fitting the experimental result with Eq. (1), we can estimate the amplitude Φ_s. For this purpose, we have to measure the decay of the signal within 0.5 s. The signal flux Φ_s increases in proportion to B_{ex} in this case, too. Therefore, effort to apply the large excitation field has been done, and the field of B_{ex}=1 mT can be applied at present. As a result, as small as 4000 magnetic particles are detected with this method. This number is more than 20 times smaller than the case of the conventional optical method.

(c) Remanence measurement

When the size of the magnetic nanoparticle becomes large, the particle can keep the remanence after the large field is applied. In the experiment, large excitation field B_{ex} is applied outside the SQUID system in order to produce the remanece of the sample. Then, the remanent magnetic field of the sample is measured with the SQUID system shown in Fig. 1(b).

Unfortunately, almost all the commercial markers do not show the remanence. Dilorio et al. used the relatively large marker that shows the remanence, where the size of the polymer is 140 nm in diameter.

They detected the binding reaction between antigen and its antibody, and showed that the sensitivity is about 100 times better than the conventional method [5].

We are also developing the magnetic marker that shows the remanence. In the present case, Fe_3O_4 magnetic particle with diameter of 25 nm is embedded in the polymer whose diameter is typically 80 nm. In Fig. 4, relationship between the remanent signal and the weight of the marker is shown. In the experiment, the remanence is produced by applying the excitation field B_{ex} of about 0.1 T.

The circles show the experimental results obtained from the bare Fe_3O_4 nanoparticles. The triangles show the experimental results obtained from the marker, i.e., when the nanoparticle is embedded in the polymer. As shown, both results agree with each other. This means that magnetic property of the nanoparticles is not degraded when they are embedded in the polymer. As shown, we can detect the nanoparticles as small as 1 pg.

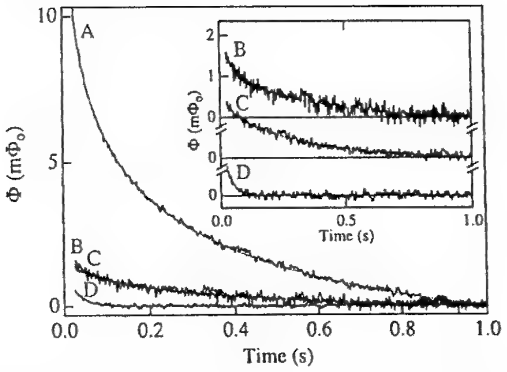

Fig. 3. Relaxation of magnetization after the excitation field B_{ex} is turned off. (ref. (4)).

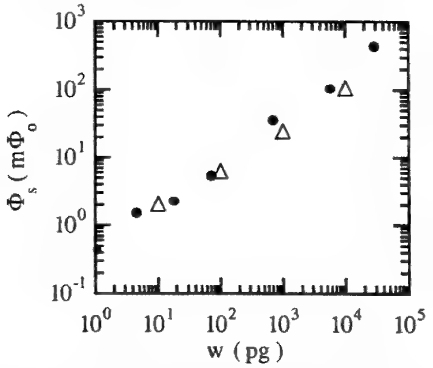

Fig. 4. Relationship between the remanent signal and the weight of 25 nm-ϕ Fe_3O_4 nanoparticles.

References

1) K. Enpuku, T. Minotani, T. Gim, Y. Kuroki, Y. Itoh, M. Yamashita, Y. Katakura and S. Kuhara, Jpn. J. Appl. Phys. **38** (1999) L1102.
2) K. Enpuku, T. Minotani, M. Hotta and A. Nakahodo, IEEE Trans. Appl. Supercond. **11** (2001) 661.
3) W. Weitschies, R. Kotitz, T. Bunte and L. Trahms, Pharm. Pharmacol. Lett. **7** (1997) 1.
4) Y. R. Chemla, H. L. Grossman, T. Poon, R. McDermott, R. Stevens, M. D. Alper and J. Clarke, Proc. National Academy of Sciences of U. S. A, **97** (2000) 14268.
5) M. S. Dilorio, K. Y. Yang, S. Yoshizumi, T. K. Nielsen and C. A. Swindlehurst, Abst. Appl. Superconductivity Conf. (Aug. 4-9, 2002, Houston U. S. A)

NMR and MRI with SQUIDs at Ultralow Magnetic Fields (J. Clarke)

John Clarke
Physics Department, University of California, Berkeley and Materials Sciences Division, Lawrence Berkeley National Laboratory, Berkeley, CA 94720

Nuclear magnetic resonance (NMR) spectroscopy in magnetic fields up to 20 T and magnetic resonance imaging (MRI), typically in a field of 1.5 T, are highly developed tools of considerable importance in chemistry, biology and medicine. The quest for ever high fields B is driven by the so-called "iron law of NMR": in thermal equilibrium the polarization is proportional to B, and the voltage induced in a coil – by Faraday's Law – scales with the NMR frequency and hence also with B. Thus, the signal amplitude is proportional to B^2. For both NMR and MRI it is highly desirable to achieve extremely narrow linewidths, typically 1 Hz for protons in liquids. This high spectral resolution at an NMR frequency of 1 GHz demands a field homogeneity of 1 part in 10^9 over the volume of the sample. Such exquisite homogeneity requires very careful shimming of the magnet. Similarly, high spatial resolution in MRI also requires a high degree of field homogeneity.

An alternative approach that offers comparable linewidths and spatial resolution at very low frequencies involves detection of the NMR signal with a dc SQUID (Superconducting QUantum Interference Device). In contrast to a Faraday detector, the SQUID responds to a magnetic flux rather than to the rate of change of flux. Thus, the signal amplitude falls off as B, rather than B^2. Furthermore, the noise temperature of a SQUID at (say) 1 kHz is a few microkelvin, many orders of magnitude below that of a semiconductor amplifier. These two attributes enable one to obtain NMR spectra of protons at frequencies as low as 100 Hz with a 1 Hz linewidth with a field homogeneity as poor as 1%.

The NMR experiments were performed with the SQUID coupled to a superconducting, second-derivative gradiometer immersed in liquid ^{4}He. The sample was inserted into a tube surrounded by the gradiometer and maintained at room temperature by means of a heater. A prepolarizing field – typically 2 mT – was applied along the axis of the gradiometer, and the static field in which the nuclei precess – with a homogeneity of about 1 part in 10^2 – was applied at right angles to the axis. To measure the NMR spectrum, the prepolarizing field was switched off, causing the nuclei to precess about the static field. An echo was formed by reversing the static field.

Figure 1 shows the NMR spectrum of 5 ml of mineral oil obtained at 1.8 mT (upper) and at 1.8 μT (lower). At the higher field, the linewidth was about 1 kHz, reflecting the field inhomogeneity. At lower field, however, the linewidth has been reduced to about 1 Hz, and the signal-to-noise ratio considerably enhanced, since the same signal power is now concentrated into a much narrower linewidth. Figure 2 shows the spectra of methanol and phosphoric acid in water and trimethyl phosphate. The electron-mediated scalar coupling of the nine protons to the ^{31}P nucleus splits the proton resonance into a doublet; the splitting is 10.4 ± 0.6 Hz.

To perform MRI, the same detector was placed at the center of a 2-m cube on which three orthogonal Helmholtz pairs were wound. These coils were used to cancel the earth's magnetic field. Two more coils supplied a polarizing field and a measurement field, and three sets of gradiometer coils provided diagonal gradients. The sample was placed outside and just below the fiberglass cryostat. This system was used to image a phantom consisting of 9 columns of mineral oil, 6 mm in diameter, arranged in a square lattice. Good quality images were obtained with resolution of about 1 mm. The MRI system is currently being modified to achieve a higher signal-to-noise ratio. Possible applications will be discussed.

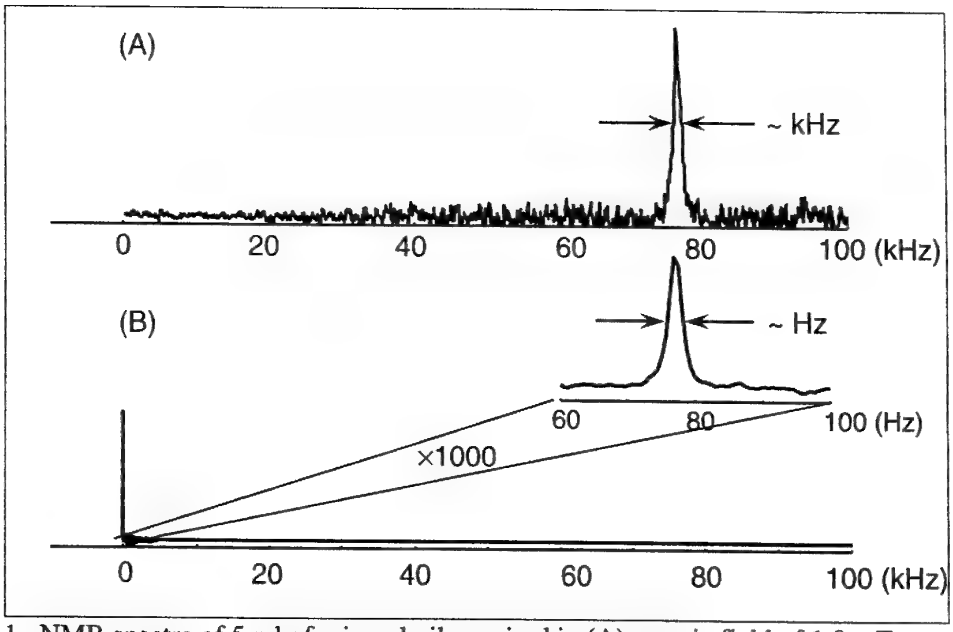

Fig. 1. NMR spectra of 5 ml of mineral oil acquired in (A) a static field of 1.8 mT, averaged over 10,000 transients, and (B) a static field of 1.8 μT, averaged over 100 transients.

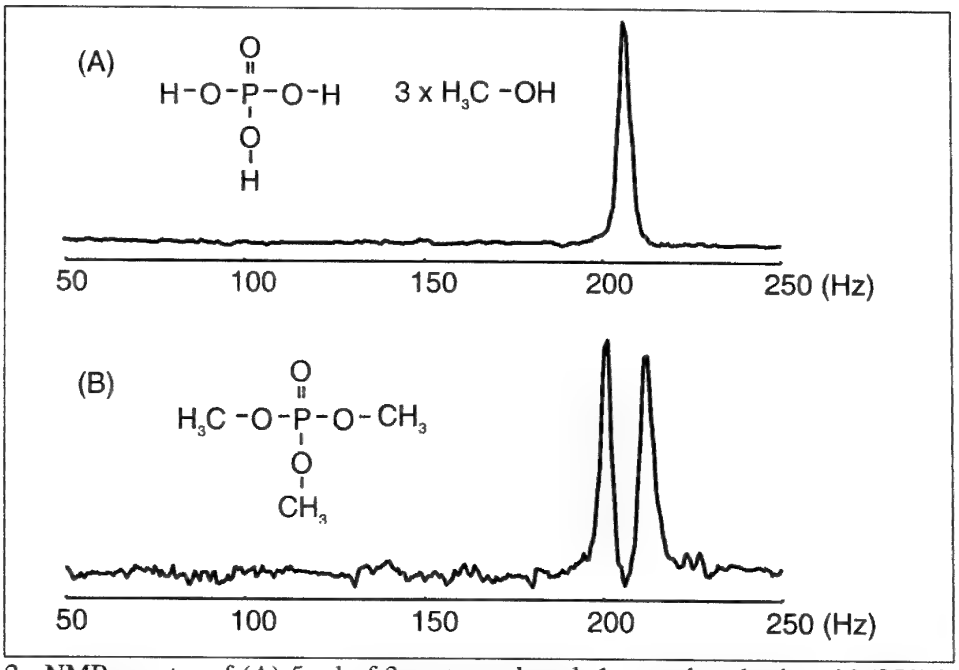

Fig. 2. NMR spectra of (A) 5 ml of 3 parts methanol, 1 part phosphoric acid (85% in water) measured at 4.8 μT, averaged over 100 transients, and (B) 3 ml of neat trimethyl phosphate measured at 4.8 μT, averaged over 100 transients.

This research was performed in collaboration with Robert McDermott, Andreas H. Trabesinger, Michael Mück, Erwin L. Hahn, and Alexander Pines and supported by the Director, Office of Science, Office of Basic Energy Sciences, Division of Materials Sciences and Engineering of the U.S. Department of Energy under Contract No. DE-AC03-76SF00098.

Metrological applications (F. Piquemal)

Active Shielding to Reduce Low Frequency Disturbances (H. Nowak)

H. Nowak
Jena SQUID GmbH, D-07751 Jena-Münchenroda

Measurements of DC near magnetic fields are disturbed by low frequency noise that is not reduced sufficiently by most of the magnetically shielded rooms or gradiometers. This can be shown in the case of biomagnetic fields very descriptively.
The biomagnetic fields are several orders of magnitude weaker than the earth´s magnetic field or the environmental noise provided by cars, trains or electrical devices. External magnetic fields are very disturbing for Magnetoencephalography (MEG) or Magnetocardiography (MCG) (analogous to Electroencephalography EEG and Electrocardiography ECG, respectively), but may be reduced successfully by magnetic shielding with material of high permeability (Mumetal) as well as by high order gradiometers [1,2].
Therefore, biomagnetic measurements are performed mostly inside walk-in shielded rooms consisting of one or more layers of Mumetal and a layer of Aluminum (Al) or Copper (Cu). The principle of this passive shielding is based either on the effect that high permeable or soft magnetic material (e.g. Mumetal) is easily remagnetized or on eddy-currents induced in high conductive material (e.g. Cu or Al).
Additionally, special antenna configurations realized in gradiometers are able to cancel homogeneous magnetic disturbing fields.
Unfortunately the shielding factor of Mumetal decreases at low frequencies, whereas the environmental noise increases. To enhance the sensitivity the recordings are done with LT_c-SQUID (Low Temperature Superconducting QUantum Interference Device) sensors cooled with liquid Helium. The magnetic noise field outside the magnetically shielded room at frequencies above 10 Hz is about 3 orders of magnitude higher than inside. Both, outside and inside the shielded room, the noise strongly increases below 2 or 3 Hz and the noise inside approaches the noise outside.
This is the reason why DC near biomagnetic measurements are usually not possible. In this case an active compensation can reduce the low frequency disturbances [3,4].
A prerequisite for an active compensation is the detection of magnetic field disturbances independent from the signal to be measured. Some active shieldings use fluxgate sensors outside the magnetically shielded room [5-8], but these methods only recognize one particular disturbing source from one direction (e.g. tram). An alternative and more potent method is the detection of disturbances as close as possible to the measuring system inside the shielded room. In such a case the sensor has to be sensitive enough to detect the disturbances inside the magnetically shielded room. The resolution of fluxgate sensors is limited to the range of some pT at more than 10 Hz, decreasing at lower frequencies. Other sensors like AMR (Anisotropic Magneto Resistance) also do not have a sufficient resolution yet. For this reason we decided to use the LT_c-SQUID technology.
Our active compensation consists of a reference SQUID measuring system positioned in the vicinity of the multichannel SQUID system for the biomagnetic measurement, pairs of Helmholtz-like coils with the axes into three orthogonal directions and a Proportional-Integral-Differential (PID) controller which is optimized for low frequencies. The signal of the reference system is proportional to the external disturbing field and is given to the PID controller that generates a current into the coils which provides an opposite magnetic field to compensate the external field.
While using the reference SQUIDs, a constant offset is added to the output signal of these sensors. This offset is compensated electronically by means of an adjustable compensation voltage. In this way the complete dynamic range of the PID controller can be used to compensate the disturbing fields.
The current through the Helmholtz-like coils and the reference signals are continuously recorded, and can be used to decide offline whether an external event or a biomagnetic signal caused a slow variation in the

data. Additionally, a signal of an external probe detecting the disturbances, e.g., a fluxgatemagnetometer was recorded.
The system has been tested by measuring the signals inside a magnetically shielded room without a subject during working hours with public traffic in the hospital area. Thus only external noise is recorded. The reference detector, a self constructed magnetometer system, is placed about 0.4m beside the measuring system. Data of a 31 channel SQUID gradiometer system (Philips, Hamburg) or a homemade 16 channel "Micro"-SQUID [9] are recorded with a spectrum analyzer (HP 3562A).
Without active shielding the environmental noise for frequencies about 20 mHz is in the order of some hundred pT, whereas with ongoing active shielding the noise is reduced to about 1 pT. At frequencies above 2 Hz the active shielding used in this setting is not effective.
In principle, it is possible to extend the frequency range of the active shielding to higher frequencies. Indeed, it has to be noted that the higher the frequency is, the greater is the phase shift of the compensation field, caused by the low pass effect of the high permeable walls.
At frequencies below 0.1 Hz the attenuation of the magnetic field is more than 50 dB, and the attenuation of the field gradient is about 25 dB. The reduction of the field gradient cannot be as sufficient as the reduction of the field because the compensation fields are generated by Helmholtz-like coils that provide a rather homogeneous magnetic field.
The shielding factor S for the magnetically shielded room Ak3b combined with the active shielding has been estimated. An external magnetic field has been generated for different frequencies and the magnetic field B_i inside the shielded room has been measured. The magnetic field B_a provided by the coil at the position of the sensor that would exist without the "yoke" of the shielded room can be calculated according to the rule of Biot-Savart. For rectangular coils this is done in [10]. In this case for low frequencies of about 50 mHz the shielding factor of the Mumetal for higher frequencies (about 80 dB at 10 Hz) has been achieved.
The improvement of the attenuation of the magnetic field disturbances is about 50 dB, the additional attenuation of the field gradient is less than 25 dB.
With this active shielding it was possible to detect DC near biomagnetic fields caused by spreading depression in animal experiments. Furthermore, the presented active shielding system enables measurements in human stroke patients in search for periinfarct depolarizations and spreading depression in migraine patients.
The system can be installed at every usual magnetically shielded room. Reference sensors inside a measuring system can be used as a feedback signal for the PID controller, so that no additional SQUID system is required.
Such an active shielding device is in principle applicable also for measurment tasks which have to be performed in unshielded environment.

Acknowledgements
This work was supported by the German BMBF under TZ-MST-VMST 16012100-16SV1272.

References
[1] J. Vrba: SQUID Gradiometers in Real Environment;in SQUID Sensors: Fundamentals, Fabrication and Applications; H. Weinstock (ed.), Kluwer Academic Publishers (1996) 117-178.
[2] H. Nowak: Biomagnetism; in Magnetism in Medicine - A Handbook; W. Andrä and H. Nowak eds.; Wiley-VCH (1998) 95-101.
[3] H.J.M. ter Brake, R. Huonker and H. Rogalla: New Results in Active Noise Compensation for Magnetically Shielded Rooms; Meas. Sci. Technol. 4 (1993) 1370-1375.
[4] D. Platzek, H. Nowak, F. Gießler, J. Röther and M. Eiselt: Active shielding to reduce low frequency disturbances in direct current near biomagnetic measurements, Rev. Sci. Instrum. 70 (5), (1999) 2465-2470.
[5] Matlashov,A., Zhuravlev,Y., Lipovich,A., Alexandrov,A., Mazaev,E., Slobodchikov,V., Wazhiewski,O.: Electronic noise supression in multichannel neuromagnetic system. In: Williamson,S.J.,

Hoke,M., Stroink,G., Kotani,M. (eds) Advances in Biomagnetism, Plenum Press, New York (1989) 725-728.
[6] Matsumoto, K., Yamagishi, Y., Wakusawa, A., Noda, T., Fujioka, K., Kuraoka,Y.: SQUID-based active shield for biomagnetic measurement. In: Hoke,M., Erné,S.N., Okada,Y.C., Romani, G.L. (eds) Biomagnetism: Clinical Aspects, Elsevier Science Publishers, Amsterdam (1992) 857-861.
[7] Urankar,L., Oppelt,R.: Design criterions for active shielding of inhomogeneous magnetic fields for biomagnetic applications. IEEE Trans. Biomed. Eng. 43(7), (1996) 697-707.
[8] Pasquarelli,A., Tenner,U., Erné,S.N.: Use of an additional active shielding system to enhance the low frequency performances of a magnetic shieldedd room. Proceedings 43rd International Scientific Colloquium, Technical University of Ilmenau, September 21-24 (1998) 123-128.
[9] Nowak ,H., Gießler, F., Huonker,R., Haueisen,J., Röther, J. and Eiselt, M.: A 16-channel SQUID-device for biomagnetic investigations of small objects. Med. Eng. & Phys., 21 (1999) 563-568.
[10] B. Weber: Electromagnetic fields. Theory and applications. Volume I - Mapping of fields; John Wiley & Sons, New York, (1954).

Others Applications (A. Platil)

A.Platil, P.Ripka
Czech Technical University, Faculty of El. Engineering
Technicka 2, 166 27 Prague, Czech Republic

In addition to previously discussed topics, magnetic sensors can be used in many other fields, such as navigation, aerospace, military and automotive. This contribution briefly summarizes the main applications.

NAVIGATION

Even today, in the age of GPS, magnetic navigation instruments are still a viable alternative, or rather a supplement to navigation systems. Such devices can provide a backup in navigation systems for the case of temporary loss of GPS signal. Traditionally, fluxgate compasses with single core and two-windings were used. These solid-state sensors provide a clear advantage over moving needle devices (vibration immunity). In recent years, cheap AMR compasses for small aircrafts are available with acceptable parameters (Honeywell).

MILITARY APPLICATIONS

The unexploded ordnance (UXO) is a serious problem in some areas, such as military air training ranges or in many European cities that experienced heavy bombing during WW2. The magnetic signature of the UXO is typically small (air bombs are demagnetized by ground impact) and depends rather on the outer dimensions and volume then on the ferrous content. Magnetic mapping of the examined area is usually used. There are some commercially available magnetic detection systems, such as the Dimads by Schiebel. These systems contain proton, Overhauser or Cesium vapor magnetometers or fluxgate sensors in gradiometric arrangement. The fluxgates provide the required sensitivity while they can operate in the field conditions, without cryogenics (unlike Squids). The gradiometer suppresses the influence of relatively high background field (Earth's field, distant sources) and the high sensitivity to local variations (signature of the ferromagnetic object) is sustained.

SECURITY

Another application is the detection of magnetically attached explosive devices (under-car booby traps). A mesh of magnetic sensors on the underneath of a car monitors the magnetic situation during parking and if suspicious changes are detected, the driver receives a warning before starting the car. The problem is to distinguish normal field changes (e.g. passage of another car with strong magnetic signature) from really dangerous activities, because unacceptably high rate of false-positive alarms would render the system unusable.

AUTOMOTIVE

Magnetic devices are often used in the industry as position sensors. Their important advantage over optical or contact sensors is the immunity to dirt and wearing. A typical application is the sensing of teeth position of ferrous cogwheel. Traditionally a Hall sensor with back-bias permanent magnet was used. Nowadays, with the developments in magnetoresistors, AMRs and GMRs penetrate this application area. Worth a short note is an interesting device, smart Hall sensor of HAL 1000 family from Micronas. It behaves like normal three-pin analogue Hall switch. However, under increased supply voltage, the internal communication interface is activated and the sensor can set or transmit its internal digital parameters, like

ADC reading, switching hysteresis (%FS) or linear and quadratic terms of its internal temperature compensation. (Temperature requirements are among the most limiting factors in automotive applications.)

TARGET DETECTION

Magnetic sensors built into the roadway are used to detect vehicles in traffic control systems. From the signal, the type of car (personal or truck) can be estimated. Submarine detection can be realized by arrays of fluxgate sensors. They are sensitive even to small gradients because they are kept at constant temperature and can be made long enough.

ANTITHEFT

Goods in shops and similar items are often labeled with security tags. Many types work on magnetic principle (electromagnetic antenna resonators, Wiegand wire). They must provide specific response and easy deactivation (e.g. by demagnetizing the magnetically hard part of Wiegand wire).

CONTACTLESS CURRENT SENSING

Magnetic sensors (e.g. AMRs) can be used for contactless current sensing. If more than one sensor is used, the influence of interfering field can be compensated. Sometimes, an arrangement with ferromagnetic core and feedback is used for better accuracy.

REFERENCES

[1] P. Ripka (ed.): Magnetic Sensors and Magnetometers, Artech House Publ., ISBN 1-58053-057-5

[2] http://www.honeywell.com

[3] http://www.schiebel.com

[4] R. K. Jurgen: Automotive Electronics Handbook, McGraw-Hill, ISBN 0-07-034453-1

[5] D. Dwyer: A Self-Calibrating Miniature Hall Effect Solution to Gear Tooth Speed Sensing, Sensors Magazine, Vol.18, No.9 (Sep. 2001), p.14-24.

[6] http://www.micronas.com/

[7] G. Herzer: Magnetic materials for electronic article surveillance. J. Magnetism and Magnetic Materials, article in press, fall 2002.

[8] General Magnetic Sensors – Data sheet http://www.philips.semiconductors.com

Magnetic Microscopy using SUID sensors (F. Baudenbacher)

Franz Baudenbacher

Superconducting QUantum Interference Device (SQUID) magnetometers have unsurpassed energy sensitivity and have been used to provide images of the magnetic field distributions associated with nerve and muscle action currents, development currents in the chick embryo, remnant magnetization in geological thin sections, currents in integrated circuits, trapped flux in superconductors, motion of magnetotactic bacteria, cracks and defects in metals, ongoing corrosion activity, and Johnson noise. The aim of the lecture is to provide an overview of applications of SQUID microscopy with a particular focus in biomagnetism and geomagnetism.

A central question in biomagnetism is how biomagnetic fields are generated and if biomagnetic fields can contain information not present in the bioelectric potential. The focus of the tutorial is partly on cardiac electrophysiology, especially the relationship between the electrocardiogram and the magnetocardiogram and possible clinical applications of the MCG.

Current geomagnetic SQUID based instrumentation which measure magnetizations are limited in sensitivity and can only be used on homogeneous samples and fail if the sample carries a heterogeneous magnetization.

Since the nature of the magnetic field in geological samples is different compared to biomagnetic sources the requirements for the SQUID sensors are different. The lecture will discuss the requirements on spatial resolutions and field sensitivity and describe the trade offs of different sensor geometries as well as a common cryogenic platform for a configurable SQUID microscope.

List of speakers

Speakers	Address	E-mail
Pr. Pavel Ripka	Department of Measurement Faculty of Electrical Engineering Czech Technical University Technicka 2 166 27 Praha 6 Czech Republic	ripka@feld.cvut.cz
Pr. Christophe Dolabdjian	GREYC UMR 6072 6, Bd du Maréchal Juin F-14050 CAEN Cedex	c.dolabdjian@greyc.ismra.fr
Dr. Jiri Vrba	CTF Systems Inc., A subsidiary of VSM MedTech Ltd. 15-1750 McLean Ave., Port Coquitlam, B.C. Canada V3C 1M9	jvrba@ctf.com
Dr. J.M. Léger	CEA-Direction de la Recherche Technologique LETI/DSIS/SSIT 17 rue des Martyrs F38054 Grenoble Cedex 9	Leger@chartreuse.cea.fr
Pr. Andriy Yashan	Fraunhofer IZFP University, B. 37 66123 Saarbruecken Germany	Andre.Yashan@izfp.fraunhofer.de
Dr. Fritz Primdahl	Danish Space Research Institute Juliane Maries Vej. 30 DK-2100 Copenhagen Oe, Denmark	fpr@oersted.dtu.dk
Dr. Vincent Mosser	SchlumbergerSema Utilities Montrouge Technology Group 50 avenue Jean Jaurès BP 620-13, F-92542 Montrouge	mosser@montrouge.sema.slb.com
Pr. Petr Nikitin	General Physics Institute Academy of sciences of Russia 38, Vavilov St, Moscow 117942, Russia	nikitin@kapella.gpi.ru
Pr. Meinhard Schilling	Institut für Elektrische Meßtechnik und Grundlagen der Elektrotechnik Hans-Sommer-Straße 66, D-38106 Braunschweig	m.schilling@tu-bs.de
Dr. Larissa Panina	CRIST Research Group University of Plymouth, Plymouth PL4 8AA England	L.Panina@plymouth.ac.uk
Pr. S. Tumanski	Warsaw University of Technology Institute of Electrical Theory and Measurements - IETiME Koszykowa 75, 00-661 Warszawa Poland	slawomir.tumanski@inetia.pl
Dr. Stéphane Flament	GREYC -CNRS UMR6072 6, Bd du Maréchal Juin 14050 Caen Cedex France	s.flament@greyc.ismra.fr
Dr. Franz Baudenbacher	Department of Physics and Astronomy, Vanderbilt University 6301 Stevenson Center, Box 1807 Station B Nashville, TN 37235, USA	F.Baudenbacher@Vanderbilt.edu
Dr. Marc Lam Chok Sing	GREYC -CNRS UMR 6072 6, Bd du Maréchal Juin 14050 Caen Cedex France	m.lam@greyc.ismra.fr
Dr. Yann Bourez	GESMA/DDNA BP 42 29240 Brest naval France	bourez@gesma.fr
Dr. Jean Rasson	Institut Royal Meteorologique Centre de Physique du Globe B-5670 Dourbes Belgique	jr@oma.be
Dr. Marc Kreutzbruck	Marc von Kreutzbruck Institut fuer Angewandte Physi Heinrich-Buff-Ring 16, 35392 Giessen	Marc.v.Kreutzbruck@physik.uni-giessen.de
Dr. Marcel ter Brake	Group Leader Instrumentation and Cooling Department of Applied Physics - University of Twente P.O.Box 217, 7500 AE Enschede, The Netherlands	h.j.m.terBrake@tn.utwente.nl
Pr. Keiji Enpuku	Dept. of Electoronic Device Engineering, Kyushu University. Hakozaki 6-10-1, Higashi-ku, Fukuoka 812-81, JAPAN	enpuku@ed.kyushu-u.ac.jp
Pr. John Clarke	Physics Department University of California at Berkeley Berkeley, CA 94720	jclarke@physics.berkeley.edu
Dr. Francois Piquemal	BNM 96 L.C.I.E. 33, avenue du General Leclerc 92260 Fontenay aux roses France	francois.piquemal@lne.fr
Dr. Hannes Nowak	Biomagnetic Center, Department of Neurology, University Jena, Philosophenweg 3 07743 Jena, Germany	hnowak@biomag.uni-jena.de
Dr. Antonin Platil	Department of Measurement Faculty of Electrical Engineering Czech Technical University - Technicka 2 166 27 Praha 6 Czech Republic	platil@feld.cvut.cz

List of participants

Last Name	First Name	Institution	Address	Email
ALVES	Francisco	ENS Cachan	61 av. Pdt Wilson 94235 Cachan	alves@lesir.ens-cachan.fr
ANDREAS	Friedrich	SENSITEC	Gewerbestr.. 5-9, D-35633 Lahnau	andreas.friedrich@sensitec.com
AUSANIO	Giovanni	INFM	Piazzale Tecchio, 80 80125 Napoli ITALY	ausanio@tin.it
BENSETTI	Mohamed	LGEP-Supelec	Joliot Curie GIF sur Yvette 91192 Cedex	bensetti@lgep.supelec.fr
BENYOSEF	Luiz	Observatorio Nacional	Rua General Jose Cristino, 77 Sao Cristovao – 20921-400 Rio de Janeiro R.J. Brazil	benyosef@on.br
BIELLMANN	Cedrick	CEA/Saclay	CEA Saclay DRT/DCES/SISC Bat 611, 91191 Gif sur Yvette Cedex	biellman@ortolan.cea.fr
BLANCON	Rémi	Université d'Avignon et des Pays de Vaucluse	UFR Sciences 33 rue Louis Pasteur 84000 Avignon	Remi.blancon@univ-avignon.fr
BRAZDEIKIS	Audrius	University of Houston	3201 Cullen Blvd. Suite 202, TCSAM, Houston, TX 77204	audrius@uh.edi
BURLAKOVS	Juris	State Land Service of Latvia	O. Vaciesa street 43, Rigo, LV-1004, Latvia	juris.burlakovs@gp.vzd.gov.lv
CERMAN	Ales	CTU Prague	Technica 2 16627 Prague 6 CZECH Republic	xcermana@feld.cvut.cz
CHIRIAC	Horia	National institute of research and development for technical Physics	Bld Mangeron 47, Iasi Romania	hchiriac@phys-iasi.ro
CHRISTOL	Philippe	Université d'Avignon et des Pays de Vaucluse	UFR Sciences 33 rue Louis Pasteur 84000 Avignon	Philippe.Christol@univ-avignon.fr
COISSON	Marco	IEN Galileo Ferraris	strada delle Cacce 91, 10135 Torino Italy	coisson@ien.it
CREPEL	Olivier	CNES LaMIP	2 rue de la Girafe 14079 Caen Cedex 5	Olivier.Crepel@Philips.com
CZIPOTT	Peter V.	Quantum Magnetics, Inc.	7740 Kenamar Court, San Diego, CA 92121-2425, USA	Peter.czipott@qm.com
DALICHAOUCH	Yacine	Quantum Magnetics, Inc.	7740 Kenamar Court, San Diego, CA 92121 USA	yacine.dalichaouch@qm.com
DE COS	David	Basque Country University	Apt.644, 48080 Bilbao (Spain)	dce@we.lc.ehu.es
DEVOILLE	Laurent	BNM-LNE	33 avenue du Général Leclerc, 92260 Fontenay-aux-Roses	laurent.devoile@lne.fr
FESSANT	Alain	Université de Bretagne Occidentale	6 avenue Le Gorgeu	Alain.fessant@univ-brest.fr
FONG DE LOS SANTOS	Luis Enrique	Vanderbilt University	6301 Stenvenson Center, Nashville, TN, 37238, USA	luis.e.fong@vanderbilt.edu
GARCIA	Daniel	University of Salamanca (Spain)	PLZ MERCED S/N	danielgg@usal.es
GASPARICS	Antal	Research Institute for Technical Physics and Materials Science	1121 Budapest, Konkoly T.M. u. 29-33. HUNGARY	gaspari@mfa.kfki.hu
GIERAL TOWSKI	Jacek	UBO	LMB, UFR Sciences, UBO, 6 avenue Le Gorgeu, BP 809, 29285 Brest Cedex	gieral@univ-brest.fr
GILLES-PASCAUD	Catherine	CEA Saclay	CEA Saclay DRT/DCES/SISC Bat 611, 91191 Gif sur Yvette Cedex	catherine.gilles-pascaud@cea.fr
HEIM	Erik	TU Braunschweig	Hans-Sommer-Strasse 66, D-38106 Braunschweig	e.heim@tu-bs.de
HERNANDEZ	Esteban	Universidad Nacional Autonoma de Mexico	Instituto de Geofisica-UNAM. Circuito exterior s/n Ciudad Universitaria c.p. 04510 Mexico D.F., MEXICO	estebanh@tonatiuh.igeofcu.unam.mx

HIRSINGER	Laurent	Laboratoire de Mécanique Appliquée R.Chaléat	24 chemin de l'Epitaphe 25000 Besançon	laurent.hirsinger@univ-fcomte.fr
IANNOTTI	Vincenzo	INFM-UdR Napoli, Italy	Piazzale V. Tecchio 80	iannotti@na.infn.it
KAHLEN	Olaf	SENSITEC	Im Amtmann 6, D-355788 Wetzlar	olaf.kahlen@sensitec.com
JAY	Jean-Philippe	Université de Bretagne Occidentale	6 avenue le Gorgeu 29285 BREST	jay@univ-brest.fr
KASPAR	Petr			
KOKABI	Hamid	Université P. M. Curie (Paris 6)	Tour 12, 2e étage, 4 place Jussieu, 75252 Paris cedex 05	kokabi@ccr.jussieu.fr
LEMBERE	Ilze	State Land Service of Latvia	O. Vaciesa street 43, Rigo, LV-1004, Latvia	ilze.lembere@gp.vzd.gov.lv
MONTERO	Oscar	University of Salamanca (Spain)	PLZ MERCED S/N	oscarmontero@jazzfree.com
OSSART	Florence	CNRS	LMT – 61 av. du Président Wilson, 94235 Cachan Cedex	Florence.Ossart@lmt.ens-cachan.fr
PEDERSEN	Lars William	Danish Meteorological Institute	Lyngbyvej 100, DK-2100 Copenhagen Oe	lwp@dmi.dk
PLATIL	Antonin	Department of Measurement Faculty of Electrical Engineering Czech Technical University	Technicka 2 166 27 Praha 6 Czech Republic	platil@feld.cvut.cz
POIDRAS	Thierry	CNRS	um2 cco60 34095 Montpellier cedex 5	poidras@dstu.univ-montp2.fr
POULICHET	Patrick	ESIEE	2 Bd Blaise Pascal 93162 Noisy Le Grand	poulichp@esiee.fr
PREMEL	Denis	CEA/Saclay	Bat 611, 91191 Gif sur Yvette Cedex	Denis.premel@cea.fr
PULZ	Eberhard	GeoForschungsZentrum Potsdam, Germany	GeoForschungsZentrum Potsdam, Adolf-Schmidt-Observatorium, Lindenstr. 7, 14823 Niemegk, Germany	epulz@gfz-potsdam.de
QASIMI	Ahmed	GREYC	6, Bd du maréchal Juin F-14050 CAEN	Qasimi@greyc.ismra.fr
ROBBES	Didier	GREYC	6, Bd du maréchal Juin F-14050 CAEN	D.Robbes@greyc.ismra.fr
SALOMONSKI	Nizan	R&D Integrated system SOREQ NRC	YAVNE 81800 ISRAEL	nizanf@soreq.gouv.il
SANEITR	Jiri	Department of Measurement Faculty of Electrical Engineering Czech Technical University	Technicka 2 166 27 Praha 6 Czech Republic	saneitr@feld.cvut.cz
SCORRETI	Riccardo	Ecole Centrale de Lyon	36, avenue Guy de Coloongue, 69131 Ecully	rscorret@canmet.it
SKUPUNSKI	Marek	The Angstrom Laboratory, Uppsala University	Dept of material sciences Box 534 SE 751 21 Uppsala	marek.skupinski@angstrom.uu.se
STELKA	Hana	Department of Measurement Faculty of Electrical Engineering Czech Technical University	Technicka 2 166 27 Praha 6 Czech Republic	stelka@feld.cvut.cz
TIPEK	Alois	Department of Measurement Faculty of Electrical Engineering Czech Technical University	Technicka 2 166 27 Praha 6 Czech Republic	tipek@feld.cvut.cz
VALAVANOGLOU	Aris	Space research institute of the Austria academy of sciences	Dept of experimental space research Schmiedlstr. 6 8042 GRAZ AUSTRIA	Aris.valavanoglou@oeaw.ac.at
VALENTINO	Massimo	INFM	Piazzole V. Tecchio 84	valentin@unina.it
VERWEERD	Arre	Forschungszentrum Jülich	52426 Jülich, Germany	a.verweerd@fz-juelich.de